National Transportation Safety Board
Office of Research and Engineering
Washington, DC 20594

RRD22LR001

MATERIALS LABORATORY

Specialist's Factual Report 22-032

September 21, 2022

(This page intentionally left blank)

A. ACCIDENT INFORMATION

Location: Arlington, Virginia
Date: October 12, 2021
Time: 4:50pm eastern daylight time
14:15 coordinated universal time
Vehicle: WMATA Metro Blue Line
Investigator: Joe Gordon, RPH-10

B. COMPONENTS EXAMINED

Disassembled wheelset wheels and axles
Remnants of brake rotors
Gearbox

C. EXAMINATION PARTICIPANTS

Specialist Erik Mueller, Ph.D., P.E.
Office of Research and Engineering – Materials Laboratory Division
NTSB

D. DETAILS OF THE EXAMINATION

On October 12, 2021, at about 4:50 pm local time, outbound Washington Metropolitan Area Transit Authority (WMATA) Metrorail train 407 derailed between the Rosslyn and Arlington Cemetery stations. The train was traveling southbound on track No. 2 of WMATA's Blue line toward Franconia-Springfield. There were 187 passengers onboard, and one passenger was transported to hospital.

The train consisted of eight 7000 series cars. The operator initially reported a stuck brake on car 7200, but upon inspection, it was determined that the fourth axle on car 7200 (fourth car from the head end) had derailed. Based on the direction of travel, the derailed wheelset was the lead axle of the lead truck. After the derailment, the train traveled approximately 1800 feet before coming to a stop in the tunnel, remaining upright and in line.

Broken sections of brake discs were identified in this area and were sent to the NTSB Materials Laboratory. In addition, over the course of the investigation, several wheels and axles from the derailed train cars were also sent to the NTSB Materials Laboratory.

The accident car, S/N 7200, was a four-axle lead or A car, attached or 'married' to a second car with S/N 7201. The wheelset that derailed had been assembled April 8,

2016 at ORX (Tipton, PA).[1] From the wheelset of concern, the axle (S/N 1352 or 001352) was forged in October 2015 at Nippon Steel & Sumitomo Metals per AAR M-101 Class H.[2,3] The wheel on the left side (LS) of the axle, also called the gearbox side (GS) or S-Side wheel, had S/N 2833 and was forged October 2015 at Osaka, Japan. The opposite right side (RS) wheel, also called the motor side (MS) or T-Side wheel, had S/N 2841 and was forged at the same month and location as the LS wheel. Both these wheels were classified as and manufactured according to AAR M-107 Class C specifications.[4]

When pressed on at ORX, the mounting force on the RS wheel was 64 tons with a 30-ton spike, at an interference of 0.0044 in (4.4 mils). The mounting force on the LS wheel was 58 tons with a 27-ton spike and an interference of 0.0044 inches. The weather on the date of assembly was 30 to 43 °F with no precipitation, and a 27 °F dew point at 28.41 inHg.[5] Wheels mounted by ORX are typically temperature stabilized and assembled in a 20 °C (68 °F) climate-controlled environment.

1.0 On Scene Disassembly at WMATA Greenbelt

NTSB personnel were present at the WMATA Greenbelt facility on October 20, 2021 to witness the disassembly of the aforementioned #4 axle (#001352) wheelset.

Prior to removal, the wheels on the #4 axle were examined. While the inside face of the wheel hub should be flush against the bearing when pressed on the wheel seat, there was a gap on both the right side (RS) and left side (LS) wheels. Figure 1 shows the gap on the RS wheel, and the gap on the LS wheel is shown in Figure 2.

The gap on the LS side was approximately 0.63 inches (16 mm) and the gap on the RS side was approximately 1.10 inches (28 mm). In addition, the outer face of the axle seat typically sits outboard of the outer wheel face. As shown in Figure 3 and Figure 4 for the LS and RS, respectively, the axle face was flush with that of the LS wheel, and it was recessed on the RS wheel. This recession was measured as 0.94 inches (24 mm). The stated back to back measurement, or measurement between the inside faces of the wheels, was 55.3125 inches, or about 2 inches wider than the 53 5/16 ±1/16 inch requirement.

---

[1] ORX is a railroad products company headquartered in Tipton PA, and is a party to the investigation.
[2] Nippon Steel & Sumitomo Metals, now Nippon Steel Corporation, is a steel and iron products company headquartered in Tokyo, Japan. The markings on the wheels and axles indicated manufacture in Osaka, Japan.
[3] AAR M-101, Class H describes a carbon steel axle material that has been normalized, quenched, and tempered.
[4] AAR M-107, Class C describes a carbon steel wheel material that has been forged, heat treated, and rim-quenched at a subcritical temperature.
[5] Weather Underground, for Tipton, PA on April 8, 2016

The wheels were removed using a specialized press machine, first removing the RS wheel, then removing the LS wheel. Upon removing the LS wheel, a small piece of the wheel was observed falling out. This piece was retained by the NTSB Materials Laboratory, and it was later found to exhibit features consistent with arcing damage and overstress fracture.

Figure 5 shows part of the surface of the RS wheel seat of the axle, after removal of the respective wheel. Figure 6 shows the wheel seat of the LS wheel. Both axle seat surfaces exhibited longitudinal streaks and gouges; the degree of damage was more widespread and deeper on the LS wheel seat surface. These features indicated material transfer between the inner bore surface of the wheels and the outer surface of the axle wheel seat, consistent with material galling.

Figure 6 also shows an irregular pattern to the surface oxidation, or rust, layer. This layer was consistent with water or humid air intrusion between this wheel and axle mating surfaces. Several areas of the rim from the removed LS wheel exhibited damage, as typified in Figure 7 and Figure 8. The damage in Figure 8 was consistent with a fracture surface.

2.0 Wheelset Disassembly at ORX Facility

Parties to the investigation met in Tipton, PA at the ORX facilities in October 2021 to witness the measurements and decoupling of six (6) additional wheelsets. Three of the wheelsets had been removed from service since the back-to-back inspections following the accident, and three more had been removed prior to the accident, but since 2017 (referred to as 'historical' wheelsets). The three wheelsets that were removed from service after the accident came from cars 7180, 7344, and 7165. One of the wheelsets is depicted in Figure 9.

Prior to disassembly, a variety of measurements were taken, including:

- Radial runout on tread of the wheels
- Axial runout on back rim face of the wheels
- Back-to-back measurements at three 120° locations
- Axle projection beyond front wheel hub face at two 90° locations
- The gap (if present) between the bearing seal ring and wheel back hub face for both wheels

During disassembly, the following were measured:

- Force required to break wheel from its interference fit, or static friction (tons)
- Force required to smoothly move the wheel from its seat, or kinetic friction (tons)
- Sound produced when breaking the wheel from its fit (qualitative)

After removal of the wheels, the following measurements were recorded:

- Wheels
    - Rim thickness
    - Flange thickness
    - Flange height
    - Bore inside diameter, measured with a 3-pt micrometer at 3 depth locations
    - Roughness measurements of bore (R_a, R_{sk}, R_q, R_{ku}, etc.)
- Axles
    - Wheelseat outside diameter at three locations, each rotated 90°
    - Wheelseat surface roughness (R_a, R_{sk}, R_q, R_{ku}, etc.)
- Bearings and gearboxes
    - Endplay, or moveable length of bearings along axle
    - Distance between the outboard seal ring faces of the two bearings
    - End of axle gearbox to quill face
    - End of axle to outboard face of bearing seal ring

Of note were the gap measurements prior to the axle removal. These varied from 0.063 in to 0.502 inch, located on the left side (S-side) where the gearbox was located. There were no gaps measured on the opposite right side (T-side) wheels.

Figure 10 shows the bore of one of the disassembled wheels. Figure 11 shows the view of the edge of the mating axle, exhibiting a circumferential wear area about 0.68 inches in width, consistent with the protruding end of the axle wheel seat past the wheel face. Figure 12 shows the angled view, which also demonstrates the longitudinal marks on the axle wheel seat consistent with scoring wear scars against the wheel bore during disassembly.

3.0 As-Received Materials Laboratory Components

The NTSB Materials Laboratory received the wheels and axles from three wheelsets. The wheelset axles were serial numbers 1352 (the derailed wheelset in the accident), 1969, and 1345. The wheels had been pressed off the axles and strapped to wooden pallets prior to receipt. Figure 13 shows the right and left side wheels from wheelset axle 1969, Figure 14 shows the wheels from axle 1345, and Figure 15 shows the opposite wheels from the accident wheelset axle 1352.

Though the wheels were shipped on separate pallets, all the axles were shipped together in one crate, as illustrated in Figure 16. While the two axles in the upper portion of the figure are shown as disassembled, the wheel seats of the accident axle, on the bottom of the figure, had been ground to facilitate dimensional measurements by WMATA.

Figure 17 shows the wheel seat and the bearing journal of the left, or gearbox, side of the accident axle. These surfaces exhibited wear patterns consistent with their use in service—the wheel seat exhibited reflective chatter marks from the post-disassembly grinding, and the bearing journal exhibited two circumferential bands, consistent with rotation of the bearing.

Towards the inboard or right direction are the seats for the gear box (Figure 18). These surfaces show the ground ring seat and the larger gear or quill seat of the gearbox. These surfaces exhibited circumferential wear marks consistent with rotational contact in service—there were no indications of abrasion, gouging, or spalling on the surface.

Towards the right end of the axles are the journal surfaces for the right side bearing and wheel seat (Figure 19 and Figure 20, respectively). These journal and seats show comparable wear patterns and features with those on the left side of the axle.

The wheel seats of the accident axle were examined to look for indications of erosion and possible movement. The wheel seats were cleaned using a polymer scouring pad with soapy water, then rinsed and dried with isopropyl alcohol and ethanol. Figure 21 shows a rotated view of the inboard area of the left side wheel seat, prior to cleaning, shown for comparison post-cleaning, shown in Figure 22.

There was a 0.8 inch wide band of dark oxidation or rust in this area. After cleaning, a band of damage exhibiting a dull luster and pock marks was observed (see Figure 22). Figure 23 shows a closer view of the damage. This band was 0.63 to 0.75 inches in width. While there were still the concentric machine marks present on the axle wheel seat surface, localized plastic deformation and microscopic pit-like features were observed in the area highlighted in Figure 23. As shown prior to cleaning, this region also exhibited enough oxidation to obscure the underlying surface features—these characteristics were consistent with fretting wear.

Likewise, the right side axle wheel seat exhibited similar features, as illustrated in Figure 24. Only about half of the wheel seat shown was cleaned in this figure, to demonstrate the features as received versus the underlying surface features. As shown in Figure 24 and Figure 25, there was a band with a duller surface texture, exhibiting localized plastic deformation and pit-like features. This band of fretting was approximately 0.75 inches in width. Outboard of the fretting band was an area of thin erratic gouges, oriented parallel to the axle direction. Closer examination of this region found this was consistent with entrained particles that were ground into the axle during the removal of the right side wheel.

In neither of the axle wheel seats were the bands of fretting exhibit severe enough that discernible cracks had developed. In addition, there were no indications of missing or spalled material in the areas of fretting on the axle wheel seats.

In addition, the gearbox from axle 1352 was received by the lab (see Figure 26), as well as three bearings, along with 30 oil specimens. The gearbox was sealed, and showed no indications of leakage along the seals and joints. There were no indications of impact damage or other external signatures of excessive heat exposure. Examination of the cylindrical ring and quill bores found circumferential witness marks, consistent with rotation along the axle journals. There were also some isolated longitudinal wear marks—these were continuous across the bore surfaces, indicating that they were consistent with assembly and disassembly motions.

Lastly, the brake discs from the accident wheelset were sent to the materials laboratory, as shown in Figure 27 through Figure 31. Both of the brake discs had fractured in multiple locations. One of the brake disc pieces, illustrated in Figure 31, had been found away from the derailment site. This location, along with the higher thickness of surface oxidation (rust), was consistent with it having fractured prior to the final derailment. As the discs were attached to the wheels outboard of the rest of the wheelset, they would be subject to any interaction with any external components during a derailment or loss of contact with the track.

4.0 Dimensional Measurements

As mentioned prior, the wheel flanges of the accident wheels, particularly on the left side, had exhibited localized areas of fracture as well as indications of thinning. On the left side the rim flange had thinned to 0.76 inches, with an average thickness of 0.77 inches. On the right side wheel, the flange thickness averaged 0.92 inches with a minimum of 0.91 inches. These data were below the required 1.156 inch (29.4 mm) gage point thickness for any new wheel type per AAR M-107. None of the other four wheels submitted exhibited rim flange thickness of 1 inch or less.

Using a FARO Edge portable coordinate measurement machine (CMM), the cylindricity and concentricity of the LS wheel was examined, to determine if it was out of round, or if it had been deformed because of the derailment. An illustrative example of the data is in Figure 32. The following were the measurements for the LS wheel:

- Wheel Rim
    - Diameter = 696.0 mm (27.402 in)
    - Cylindricity = 0.454 mm (0.0179 in)
- Wheel Axle Bore
    - Diameter = 142.70 mm (5.618 in)
    - Cylindricity = 0.049 mm (0.0019 in)
    - Concentricity = 0.257 mm (0.0101 in)

One of the noted features of the wheels was a circumferential wear band on the inboard face near the flanges. Among the ways these features were characterized was dimensional measurements from Reprorubber rubber replica casting negatives.[6] The replica material was applied and allowed to cure along this area of the wheel surface, then sectioned and measured using a Keyence VHX-7000 digital microscope. An example of one negative rubber section is illustrated in Figure 33, showing annotated widths of the wear ring, its depth from the inboard face, and the angle of wear. These data were tabulated in Table I.

As described in Table I, the depth of wear on the right-side wheel inboard flange was more pronounced than on the left side wheel, averaging 0.01 inches more in depth. The lengths of the wear pattern were comparable, and the angles of the wear were both below 5°.

The wheel and axle were sectioned to perform a variety of tests. The axle and wheel sections are illustrated in Figure 34 through Figure 36. One of the measurements performed was on the wheel bore surface roughness. While these data are often determined by contact stylus profilometers, the NTSB Materials Laboratory used the Keyence VHX-7000 to perform optical profilometry. The method was verified using a 25 μm (125 μinch) standard at 200X and 300X magnifications.

Figure 37 shows the sectioned surface of the LS wheel bore. This figure demonstrates the bore surface towards the outboard edge, which exhibited darker coloring and rougher surfaces. These features were consistent with the portion of the wheel that had protruded past the outboard axle face. The width of this area was 0.56 inches, consistent with the inboard gap of the axle that was rust-colored, which was measured as 0.5 inches (the entire rust and dark colored inboard gap discoloration. Towards the inboard edge, the wheel bore exhibited material gouging, consistent with material that had galled with the mating axle wheel seat surface being torn out. These features were consistent with those on the mating axle surface (see Figure 6) and the chunk of fractured material examined later.

Away from these edges, the bore surface was profiled, as typified in Figure 38. This figure shows the longitudinal direction of the wheel bore in the horizontal, with the circumferential direction oriented vertically. This view demonstrates the repeating parallel marks, consistent with the marks remaining on the surface from the machining of the bore. Multiple areas were examined, in locations away from the outboard arcing damage and the inboard galling and gouging. Figure 39 shows a typical area of how the data were presented after an optical scan, performed by stacking vertical images and interpreting the data in three dimensions. Table II shows

[6] Reprorubber® Orange Medium Body is a two component, addition cured, platinum catalyzed, hydrophobic vinyl polysiloxane thermosetting polymer manufactured by Flexbar, headquartered in Islandia, NY.

the roughness data, averaged from seven locations along the bore, in micrometers (μm) and Table III shows the roughness data in microinches (μinch). The roughness numbers listed in tables are defined as:

- R_a – the average or arithmetic mean of the height from the sampled profile
- R_q – the root-mean-square or quadratic average of the height profile
- R_v – the maximum valley depth below the average
- R_z – the maximum peak to valley height difference of the profile
- R_{sk} – the skewness, or measure of asymmetry above and below the average
- R_{ku} – the kurtosis or measure of skew in the data

Overall, the average roughness, R_a of the bore was between 3 and 6 μm (118 – 236 μinch), with the root-mean squared roughness being consistent to the average at 4 – 7 μm (157 – 267 μinch).

5.0 Mechanical and Chemical Properties Tested

The accident axle and the LS wheel were sectioned to allow for further examination and testing of their chemical and mechanical properties. Figure 34 shows the section of the axle from the surface and sectioned surface. As the parties requested the wheel seat and journal surfaces not be destroyed, sectioning was performed on the noncontact region towards the right side of the axle. The LS wheel was sectioned as shown in Figure 35. While one of the areas was sent for mechanical and chemical testing, the larger section on the right in Figure 35 was retained for testing described later. This wheel head was further sectioned as illustrated in Figure 36.

Table IV and Table V list the AAR specifications for the axle and wheel from the year the wheel and axle contracts were granted. The current 2020 issue of both specifications is the AAR M-107/M-208, although the specification applicable when the wheels were manufactured was a 2011 version.

The axle and wheel sections were machined and tested at ESi Testing in Atlanta, GA.[7] The chemical compositions were inspected per ASTM E415.[8] The tensile properties were inspected per ASTM A370.[9] In addition, the fracture toughness was examined per ASTM E399.[10]

[7] Engineering Strategies, Inc. (ESi) is a consulting engineering firm located in Cobb County, GA.
[8] ASTM E415 - *Standard Test Method for Atomic Emission Vacuum Spectrometric Analysis of Carbon and Low-Alloy Steel*, ASTM International, West Conshohocken, PA
[9] ASTM A370 - *Standard Test Methods and Definitions for Mechanical Testing of Steel Products*, ASTM International, West Conshohocken, PA
[10] ASTM E399 - *Standard Test Method for Linear-Elastic Plane-Strain Fracture Toughness of Metallic Materials*, ASTM International, West Conshohocken, PA

The mechanical and chemical test results for the axle conformed with the AAR specification M-101 Grade H (see Table IV and Table V). All results exceeded requirements. For the axle, the ultimate tensile strength (σ_{UTS}) averaged 141.2 ksi, the yield strength (2% offset) averaged 115 ksi, with the percent elongation and percent reduction of area being 17.7 % and 59.3 %, respectively.

The chemical composition of the left side wheel conformed with that specified for AAR M-107 Class C. The chemical compositions of the axle and wheel are shown in Table Table V, compared with their respective requirements.

The mechanical test data were compared with those of The Class D wheel requirements, listed in Table IV. While there were no mechanical requirements for Class C wheels, benchmarking against the Class D requirements was used to see if any gross deficiencies may have occurred during manufacturing. For the wheel, σ_{UTS} averaged 171.3 ksi, the yield strength averaged 114 ksi, and the elongation and reduction of area were 16.7 % and 44.3 %, respectively. The K_{IC} fracture toughness results were found equivalent to K_Q, with one result being 43.7 ksi·(in)$^{0.5}$ and the second being 52.4 ksi·(in)$^{0.5}$.[11]

For reference, the chemical testing results for the axle and wheel against their respective requirements. Critical hardenability diameters could be calculated from these results and the grain size. For the axle, the grain size was consistent with ASTM 8, and for the wheel ASTM 5. The ideal critical hardenability diameter for the wheel was 1.67 in, with the calculated critical diameters for quenching in water and oil being 1.00 inch and 0.35 inch, respectively. For the axle, the ideal critical hardenability diameter was 5.23 in, with the calculated critical diameters for quenching in water and oil being 4.2 inch and 3.1 inch, respectively.

The cross section of the wheel tread was examined for Rockwell hardness testing, per the recommended pattern in AAR M-107. Figure 40 shows the hardness results of the wheel cross section, tested per ASTM E18.[12] In all locations, the hardness exceeded 30 HRC—the requirement for Class C wheels was 30 to 42 HRC. The hardness of the axle was also examined per ASTM E18, although no specific testing pattern is required in M-101. The axle hardness averaged 27 HRC. These data were typical for the respective compositions and heat treatments.

6.0 Examination of Fractured Flange and Wheel Fragments

Figure 42 shows the face of a fractured area of the LS wheel flanged, sectioned to be examined microscopically. As shown in the figure, most of the wheel flange tip

[11] K_Q is the conditional fracture toughness at a critical point, and K_{IC} is the plane strain fracture toughness, a material property. These values can be equivalent given specific test criteria are satisfied.
[12] ASTM E18 – *Standard Test Methods for Rockwell Hardness and Rockwell Superficial Hardness of Metallic Materials*. ASTM International, West Conshohocken, PA.

fracture surface had been destroyed from post-fracture damage. These features included smearing and batter, consistent with repeated contact with adjacent metal components, such as the track.

There were isolated areas of the fracture surface that were undamaged, and these were able to be examined using a field emission scanning electron microscope (SEM). Overall, the portions of the fracture surface comprising discernible fracture features typically exhibited dimpled rupture, as typified in Figure 43. In some areas near the edges, cleavage facets were visible (Figure 44). These features were consistent with fracture from overstress. There were no indications of features suggesting progressive or other fracture modes. The only other features present on the flange were those consistent with post-fracture damage—the area on the right in Figure 45 shows typical smearing damage to the flange fracture surface.

Figure 46 shows the chunk of material that had separated from the wheel, and galled onto the LS axle wheel seat, as shown in Figure 6. While much of the fracture surface had been obliterated, consistent with tearing and smearing between the faying surfaces, some isolated areas of the fractured piece were able to be examined for fracture features, as illustrated in Figure 47.

The features on the fracture exhibited dimpled rupture, consistent with overstress fracture, as demonstrated in Figure 48. Figure 49 shows a spherical object, exhibiting a dendritic morphology, and composition consistent with the rest of the fractured remnant, when examined in backscattered mode.[13] These characteristics were consistent with arcing occurring in this area of the axle and wheel.

7.0 Metallographic Examination

Figure 41 shows a parallel wheel cross section that was further cross sections were vacuum cold epoxy mounted, ground and polished to 0.03 μm, and etched using a 2% nital solution.[14] This allowed examination of the axle and wheel microstructures, which showed a generally equiaxed fine grained structure in the core areas away from the surfaces (Figure 50 and Figure 51, respectively).

For the axle, the microstructure exhibited a generally equiaxed grain morphology, with a comparative grain size consistent with ASTM 8 (Figure 50). The constituents exhibited a lath morphology, consistent with a tempered martensitic microstructure. These features were typical of a heat treated, quenched, and tempered steel.

[13] Backscattered electrons: SEM micrographs produced using backscattered electrons display contrast that is associated with the atomic numbers of the elements in the micrograph. Materials containing elements with higher atomic numbers visually appear lighter relative to other materials containing elements with lower atomic numbers.
[14] Nital is a solution of 2-5% concentrated nitric acid (HNO_3) in ethanol.

As shown in Figure 51, the wheel microstructure exhibited upper transformation ferrous constituents, consistent with the heat treatment discussed in AAR M-107 (these structures are sometimes called bainite or very fine pearlite). These features were typical of those for rail wheels. Consistent with other Class C wheel microstructures, the wheel exhibited an equiaxed fine grain structure, and a comparative grain size consistent with ASTM 5.

Figure 52 displays a montage of the flange and rim corner cross section, showing a differing microstructure near the surface that had been in contact with the rail. The depth of deformation was greatest in the flange, exceeding 0.25 inch, whereas along the corner the depth is only 0.10 inches. These data were consistent with the elevated microindentation hardness values, discussed later.

Both this flange surface and the inner corner surface exhibited surface martensite, consistent with high temperatures from frictional and sliding forces (Figure 53). There were some small cracks in these areas, oriented parallel to the surfaces. The flange tip also exhibited an undulating grain flow, consistent with the folded and broken surface martensite layer.

Figure 54 shows an area of the corner which also exhibited a white-colored surface layer, consistent with untempered martensite. This indicates local heating above 1340 °F (727 °C) and rapid cooling, typical of high friction or sliding contact. Some cracks were observed, but they were shallow (less than 0.005 in (0.13 mm)) and were oriented parallel to the running surface. However, this layer was small relative to the layer of grain deformation, exhibiting a maximum depth of 0.01 inches (0.25 mm).

In contrast, the contact surface exhibited a deformed microstructure, typical with cold working or work hardening from repeated rolling contact with the rail head. At low magnifications, these areas manifest as darker and finer features (Figure 52). The grain structure near the surface shows flattening and stretching, consistent with the repeated work hardening of the surface.

Figure 55 shows the locations probed using microindentation hardness, which can be used to quantify the depth of the deformed or cold-worked microstructure from wheel-rail interaction. The testing was performed per ASTM E384.[15] The data are shown in charts in Figure 56 through Figure 58, shown in Rockwell C (HRC) as converted from HV_{500} (a Vickers hardness with a 500 g load). A summary of the data is:

[15] ASTM E384 – *Standard Test Method for Knoop and Vickers Hardness of Materials*. ASTM International, West Conshohocken, PA

- Flange
    - Untempered martensite layer as high as 63 HRC
    - Deformed microstructure (> 40 HRC) to 0.275 inch depth (7.00 mm)
- Corner of Rim and Flange
    - Surface hardness as high as 53 HRC
    - Deformed microstructure (> 40 HRC) to 0.100 inch depth (2.54 mm)
- Inboard Surface
    - Surface hardness as high as 42 HRC
    - Higher hardness (> 33 HRC) to 0.005 inch depth (0.13 mm)

Hardness values in this surface layer were over 55 HRC, consistent with untempered martensite. In the deformed areas of the microstructure, the hardness values in the range of 40 to 50 HRC were consistent with cold work from service (Figure 54).

Figure 59 shows a montage of a cross section of the edge of the wheel bore with the outboard face. This area, like those in the flange and corner, exhibited a surface layer with darker contrast, consistent with smaller, deformed grains. Figure 60 shows a closer view of the edge corner, which exhibited a clumpy surface area of white contrasting material.

Figure 61 and Figure 62 show closer views of this outboard surface, with the white material highlighted. This white material, consistent with untempered martensite, was present in a protruding globule on the wheel bore face. As this was not present uniformly over the wheel surface, this material was consistent with arced deposits observed on the LS wheel in Figure 35.

There were surface areas of uniform white-contrasting martensite, as illustrated in Figure 62. This figure shows surface distorted grains, which exhibited a wavy morphology, consistent with stepwise frictional sliding and loading. These features were consistent with this section of the wheel in frictional contact with another component, such as the track.

Figure 60 shows the wheel bore cross section near the outboard wheel edge. These figures show a surface layer inconsistent with that of the interior microstructure (exhibiting a lighter contrast). This surface layer was consistent with a surface martensitic microstructure, indicative of an area that had been heated above 1340 °F (727 °C) and then cooled rapidly. There was a uniform layer just above the interior equiaxed microstructure, which measured about 0.010 to 0.012 inch (0.25 to 0.30 mm) in thickness (see Figure 64).

There were also additional layers above that—often these lumps or other undulations exhibited voids or cracks between them and the surface white layer. As shown in Figure 65, this martensitic layer exhibited a plate-like morphology, distinct from the more uniform inner regions. Both these regions differed from the equiaxed pearlitic

(and bainitic) microstructure of the wheel interior—this microstructure was consistent with that seen through the wheel. Figure 63 also shows some of the voids found in the top layer.

These features showed the outer martensite layer was consistent with ground or worn material that had redeposited on the top surface, whereas the inner martensitic layer was consistent with frictional sliding. Except for the sporadic thicker top martensite layer, the change in microstructure extended to a depth of about 0.010 inch (0.25 mm), with no transition or deeper influence on the interior microstructure of the wheel.

Away from the edge, cross sections of the wheel bore further inboard were examined, as illustrated in Figure 66. There was no deformation of the microstructure near the surface, and no significant layer of untempered martensite. When there were some indications of surface damage (see right figure), it was confined to depths of 0.0005 inches or less (13 μm). The features and degree of damage observed near the outboard edge of the wheel bore were not observed along the rest of the wheel bore inboard.

The circumferential wear on the inboard face of the wheel was also examined using metallography. The wear was present as a more reflective band, parallel to the rim around the wheel inboard faces, as demonstrated in Figure 67 and Figure 68. In these figures, the width of the worn area averaged 0.75 inch, being approximately 0.5 inches from top of the wheel flange. While this region did exhibit radial linear features, these features were inconsistent with cracks, exhibiting no depth, as demonstrated by the lack of penetration of the reproduction rubber compound.

Figure 69 and Figure 70 show the etched cross sections of the inboard face near the flange along the area of circumferential wear. In no locations were any indications of cracking or spalling observed. Like that of the running surfaces of the wheel, this inboard surface location also exhibited deformed grain flow below a surface layer consistent with untempered martensite. The underlying grains show flow towards one direction (towards the inboard direction of the wheel).

The surface martensite layer was measured as being 0.001-0.007 inches (25-170 μm) in depth. The underlying area of deformed grains was 0.010-0.012 inches (0.25-0.30 mm) in depth. These depths were consistent with the local increase in hardness, as illustrated in Figure 56.

These features indicate high temperatures from mechanical and frictional loads, such as from sliding. If the wear is consistent with repeated contact with inside guard rails, the contact is enough to locally heat and distort the wheel surface.

8.0 Oil Analysis

Multiple oil specimens were extracted from the accident wheelset axle gearbox, as well as from the other wheelsets. These specimens were compared to an exemplar Mobil Delvac 1 75W-90 sample.[16] The accident oil samples were examined visually, using Fourier Transform Infrared Spectroscopy (FTIR), and were sent to an external laboratory for total acid number, viscosity, and water content.

The oil specimens were also filtered to extract wear debris and foreign solid material in the lubricant. An initial examination using x-ray fluorescence (XRF) found indications of iron and aluminum. After cleaning the filtered material with acetone, the material was examined using energy dispersive x-ray spectroscopy (EDS) in a SEM and XRF. The filtered debris material exhibited only indications of carbon, indicating any iron or aluminum particles that may have been present were finer than the filter paper mesh size.

Figure 71 shows an overlay of several spectra from FTIR examination of oil samples. This figure illustrates the similarity in peak locations, heights, and widths of the accident oil specimens examined by the technique compared with the exemplar specimen. The close overlapping of the spectra was consistent with consistent compositions, and a lack of decomposition products, which would typically exhibit different or separate peaks in response to the infrared testing.

Analytical ferrography on the wear debris recovered from the oil in the gearbox was performed by SGS per ASTM D7690.[17,18] The laboratory concluded that "The ferrous debris consists of normal rubbing, fatigue, corrosive wear, and oxide particles." The examination also found inorganic crystalline foreign material, consistent with soil, sand, or dirt.

There were no other discrepancies or differences noted between the accident oil specimens examined and the exemplar gear oil. These observations indicate that the oil had not decomposed or deteriorated, and was not carrying large amounts of wear debris.

[16] Mobil Delvac 1 Gear Oil 75W-90 is a fully synthetic drivetrain lubricant designed for load-carrying gears, manufactured by Exxon Mobil Corporation, Spring, TX.
[17] SGS North America, Inc. is a testing, inspection, and certification company located in Naperville, IL.
[18] ASTM D7690 – *Standard Practice for Microscopic Characterization of Particles from In-Service Lubricants by Analytical Ferrography*. ASTM International, West Conshohocken, PA

Submitted by:

Erik M. Mueller
Materials Research Engineer

Table I. The locations of the left side and right side wheel, showing the measured depths, lengths, and angles of wear on the inboard face near the flange.

Wheel and Rotation	Depth of Wear (in)	Length of Wear (in)	Angle of Wear (°)
LS 0°	0.019	0.519	1.8
LS 90°	0.034	0.802	2.3
LS 180°	0.038	0.510	3.9
LS 270°	0.028	0.509	3.6
Average	*0.040*	*0.585*	*2.9*
RS 45°	0.045	0.607	4.4
RS 90°	0.044	0.654	3.8
RS 180°	0.044	0.708	4.0
RS 270°	0.028	0.379	5.0
Average	*0.030*	*0.587*	*4.3*

Table II. Roughness measurements of Wheel Bore (in micrometers)

Location	R_a	R_q	R_z	R_v	R_{sk}	R_{ku}
Outboard, Near Edge	4.76	5.64	18.53	9.99	-0.42	0.59
Outboard	5.68	6.79	23.32	12.94	-0.31	2.00
Mid Outboard	4.09	4.93	19.24	10.85	-0.41	2.35
Outboard Near Hole	4.49	5.01	15.89	8.86	-0.28	1.64
Inboard of Hole	5.22	6.28	20.95	11.38	-0.23	1.88
Mid Inboard	5.45	5.39	18.65	10.21	-0.43	1.96
Inboard Near Galling	5.63	6.74	25.64	12.68	+0.58	2.16

Table III. Roughness measurements of Wheel Bore (in microinches)

Location	R_a	R_q	R_z	R_v	R_{sk}	R_{ku}
Outboard, Near Edge	187	222	730	393	-16.5	23.2
Outboard	224	267	918	509	-12.2	78.7
Mid Outboard	161	194	757	427	-16.1	92.5
Outboard Near Hole	177	197	625	349	-11.0	64.6
Inboard of Hole	206	247	825	448	-9.06	74.0
Mid Inboard	215	212	734	402	-16.9	77.1
Inboard Near Galling	222	265	1009	499	+22.8	85.0

Table IV. Average mechanical properties from tensile and fracture toughness testing of the Wheel and Axle Specimens, compared to those of the requirements from AAR M-101/107

Specimens or Standard	Yield Strength (psi), 0.2% Offset	Ultimate Tensile Strength (psi)	Elongation after Fracture (%)	Reduction of Area (%)	K_Q (ksi*in$^{0.5}$)
AAR M101, Class H	75000	115000	16	35	
Axle	115000	141600	17.6	59.3	
AAR M-107, Class D	115000	160000	14	30	45
LS Wheel	114000	168500	16.5	43.5	43.7, 52.4

Table V. Chemical Analysis of the Wheel and Axle Specimens, compared to those of the requirements from AAR M-101/107

	C	Mn	P	S	Si	Others of Note (>0.01)
AAR M-101, Grade H		0.60-0.90	<0.045	<0.005	>0.015	
Axle Specimen	0.43	0.93	0.014	0.012	0.29	Cu 0.016, Cr 1.02, Ni 0.028, Mo 0.212, Al 0.03
AAR M-107, Class C	0.67-0.77	0.60-0.90	<0.030	0.005-0.040	0.15-1.00	
LS Wheel Specimen	0.726	0.718	0.016	0.005	0.271	Cr 0.082, Ni 0.0285, Mo 0.017, Al 0.029

Figure 1. The gap between the inboard wheel face of the LS wheel and the axle seat hub.

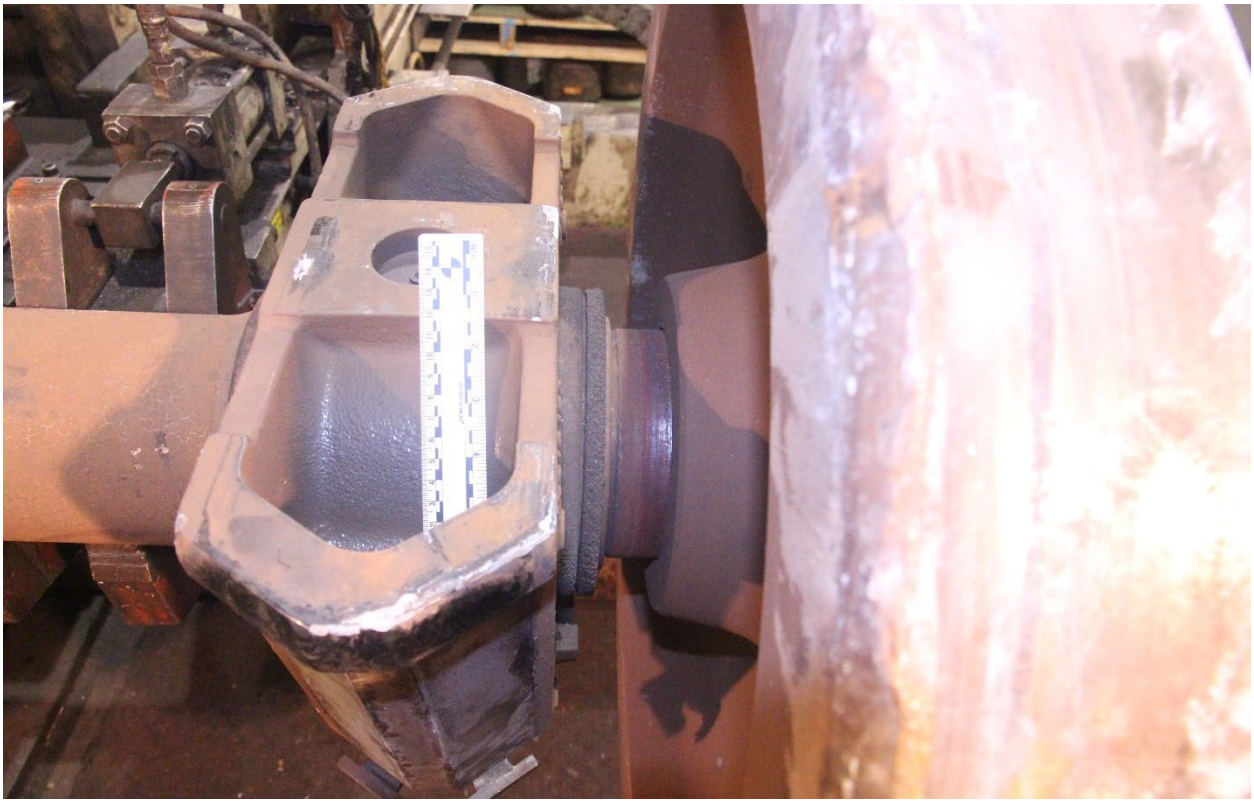

Figure 2. The gap between the inboard wheel face of the RS wheel and the axle seat hub.

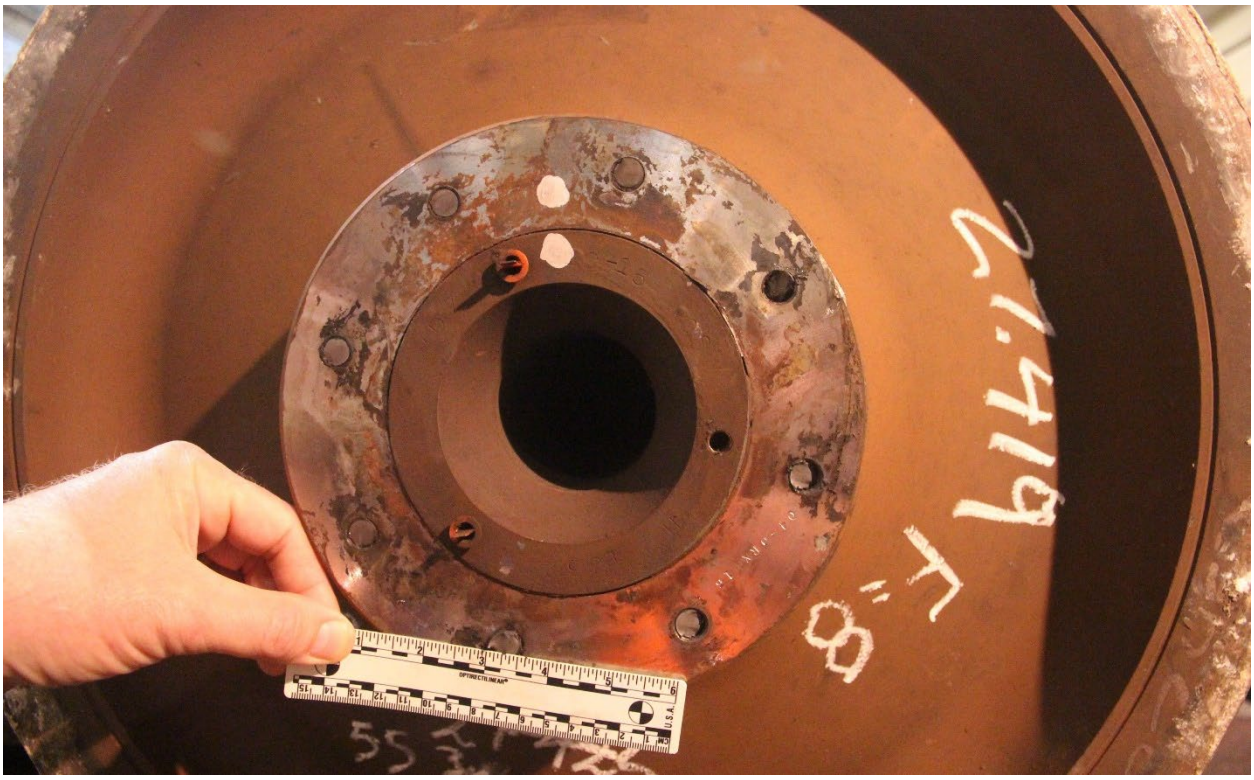

Figure 3. Outboard wheel and axle faces of the LS wheel.

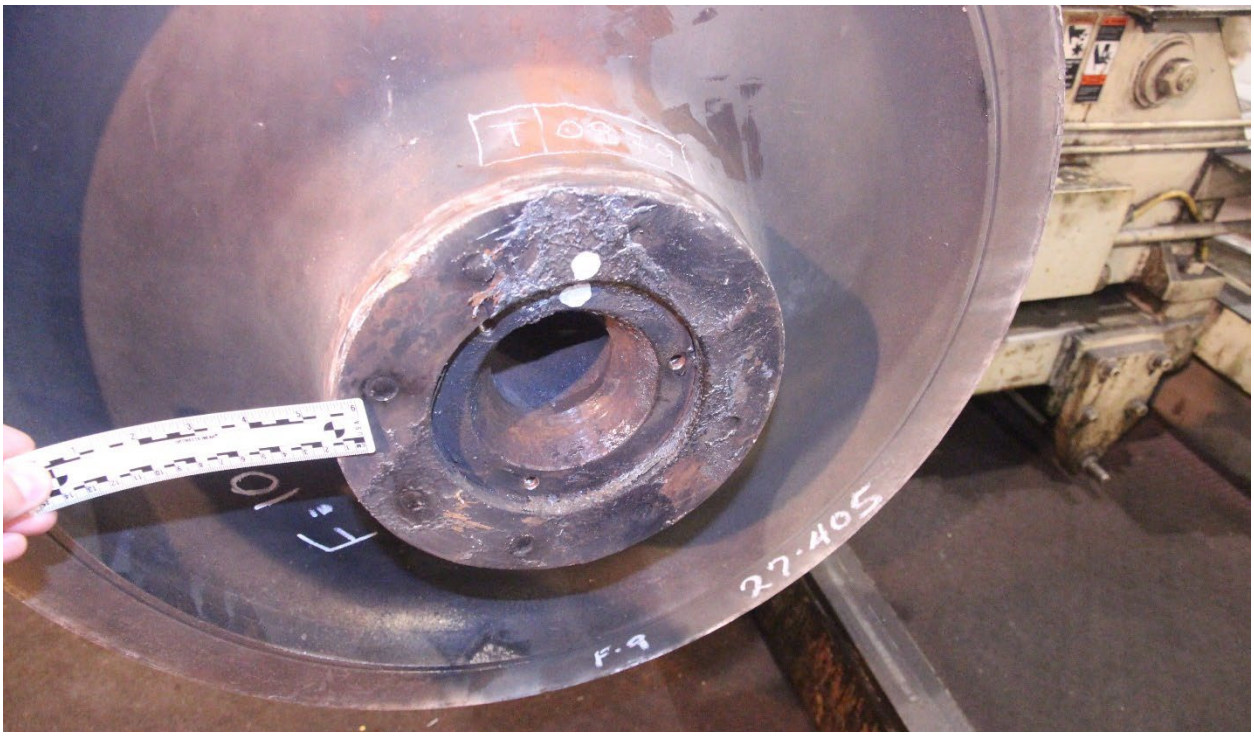

Figure 4. Outboard wheel and axle face of the RS wheel.

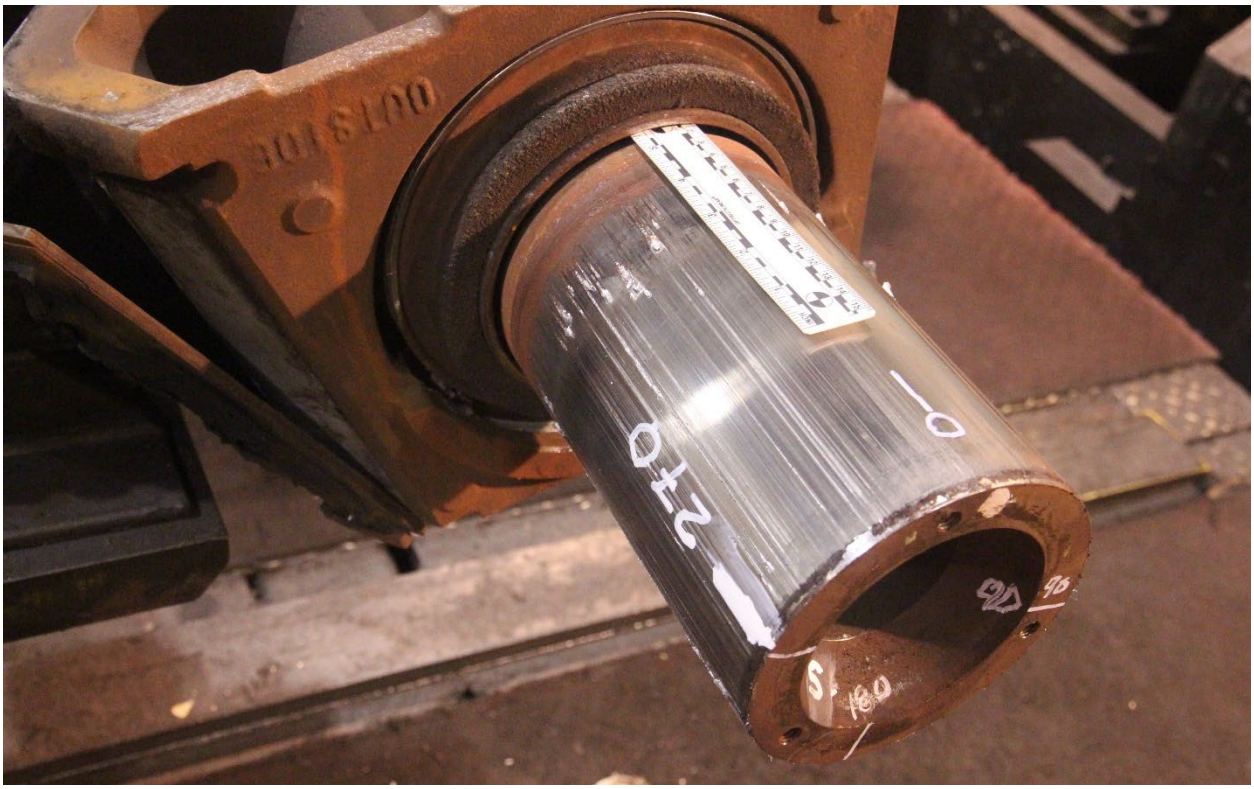

Figure 5. View of the axle seat surface after removal of the RS wheel.

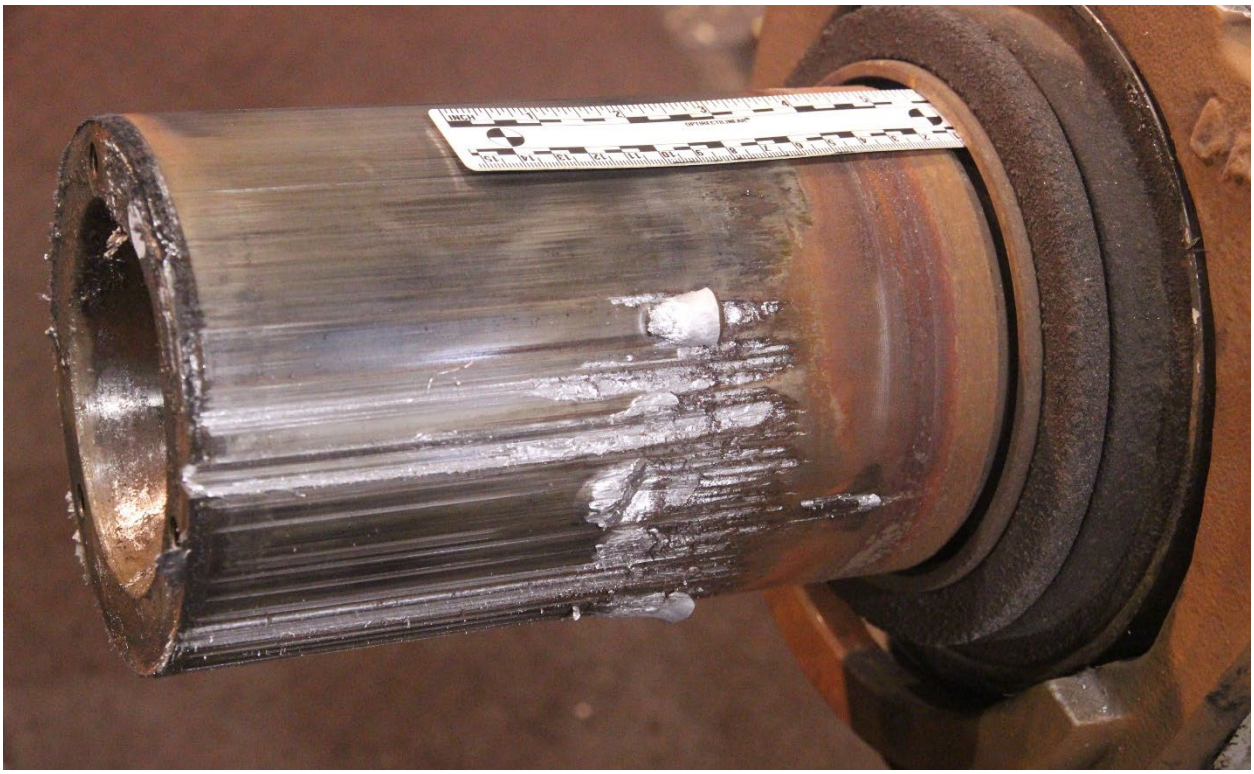

Figure 6. View of the axle seat surface after removal of the LS wheel.

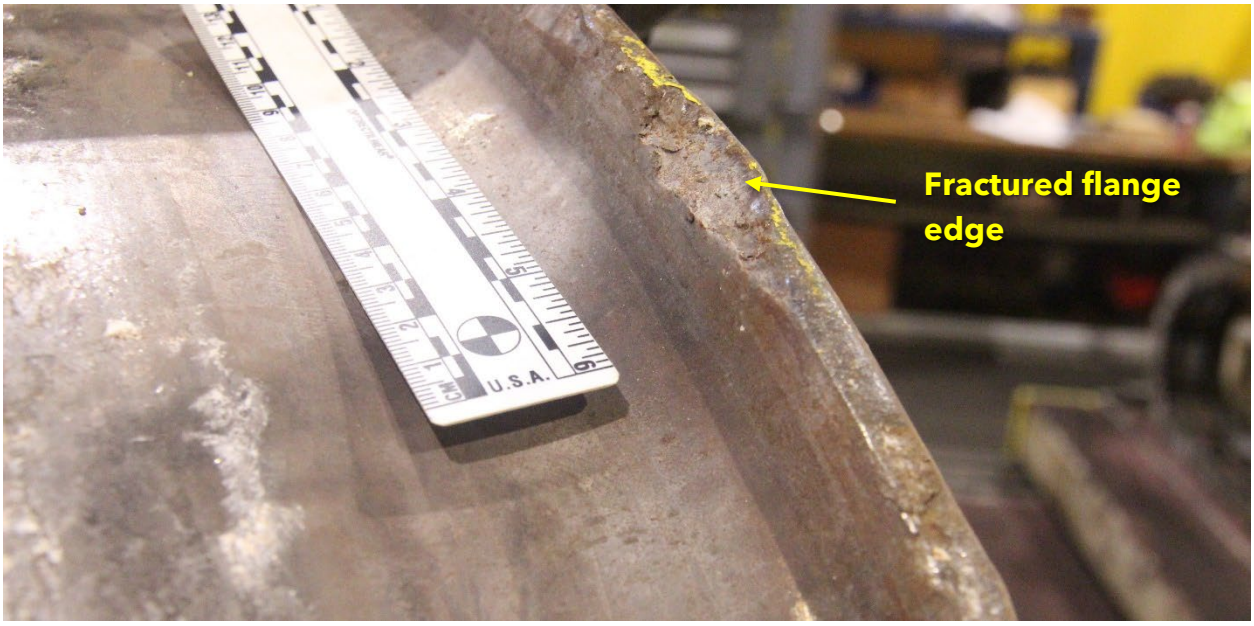

Figure 7. View of a fractured flange segment of the LS wheel rim.

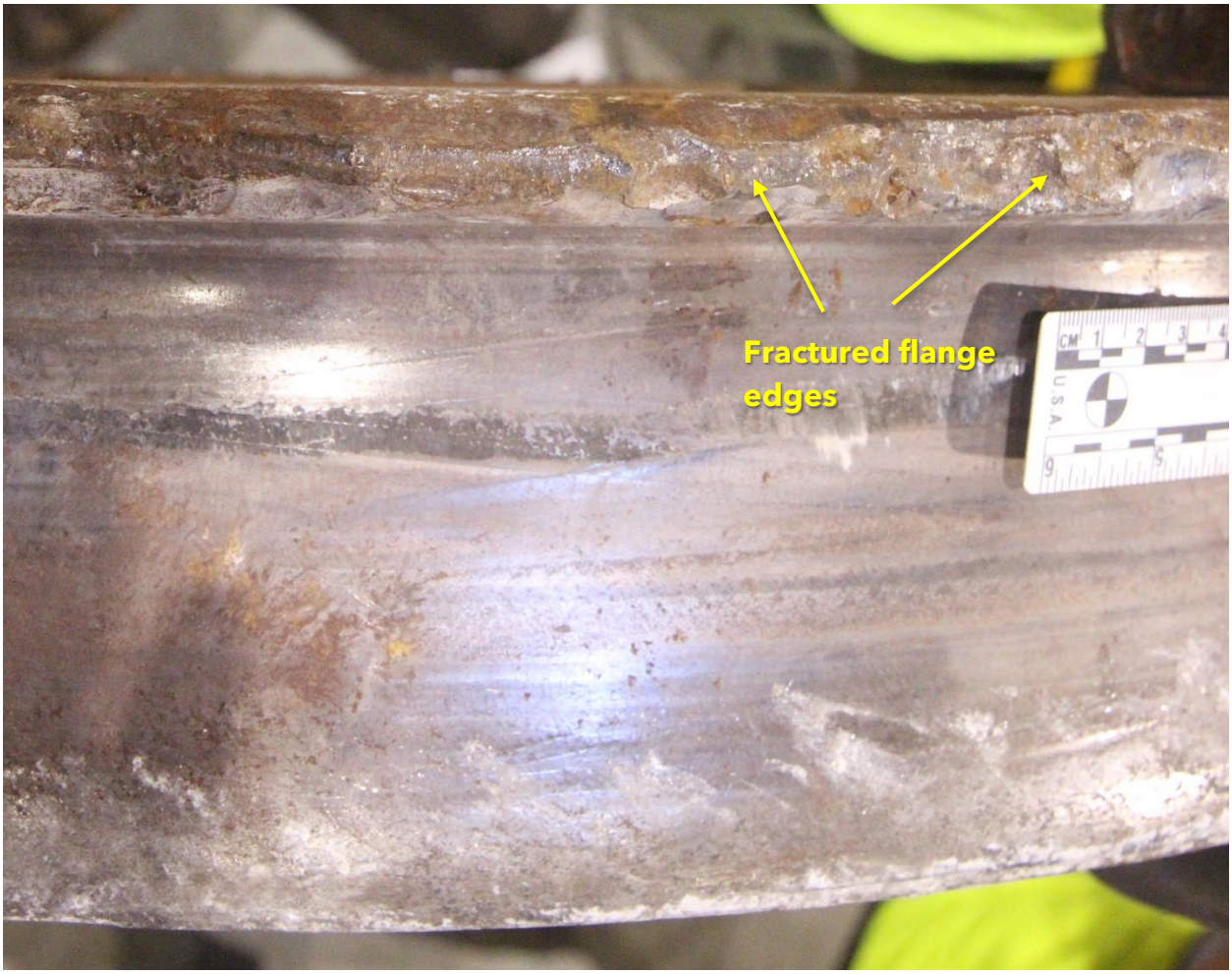

Figure 8. Additional views of damage to the rim of the LS wheel.

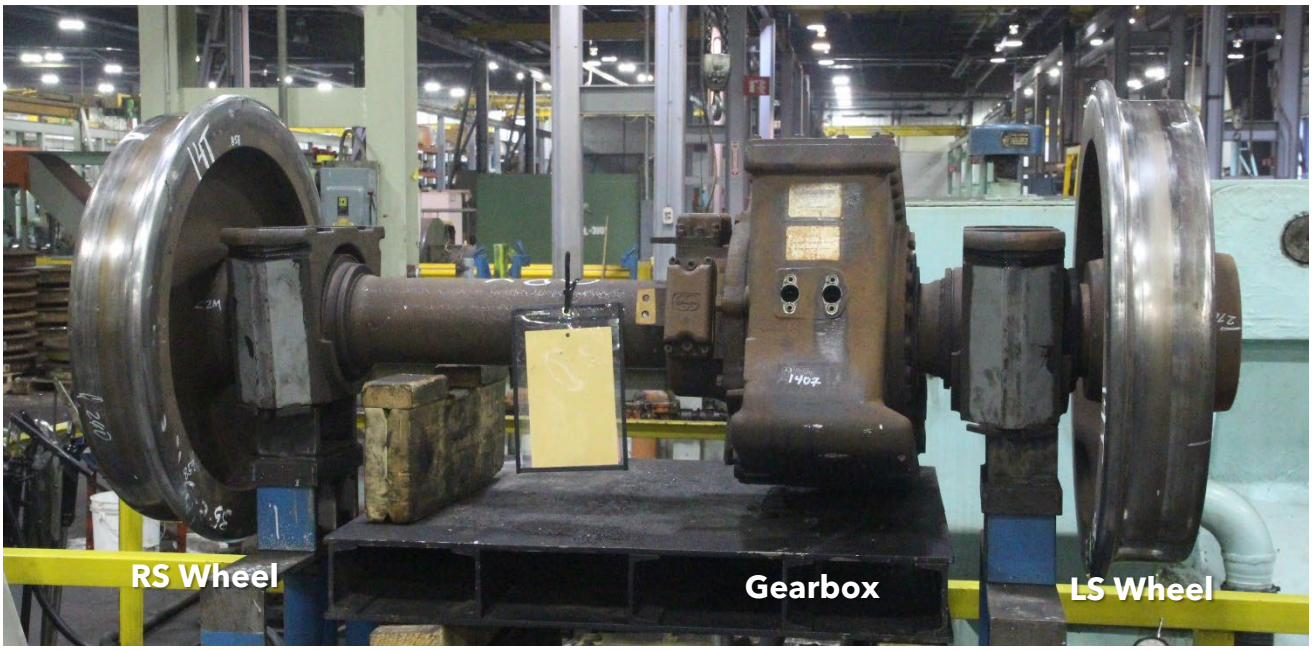

Figure 9. Wheelset from Car 7344, prior to disassembly at ORX.

Figure 10. The bore of the disassembled RS wheel S/N 2079.

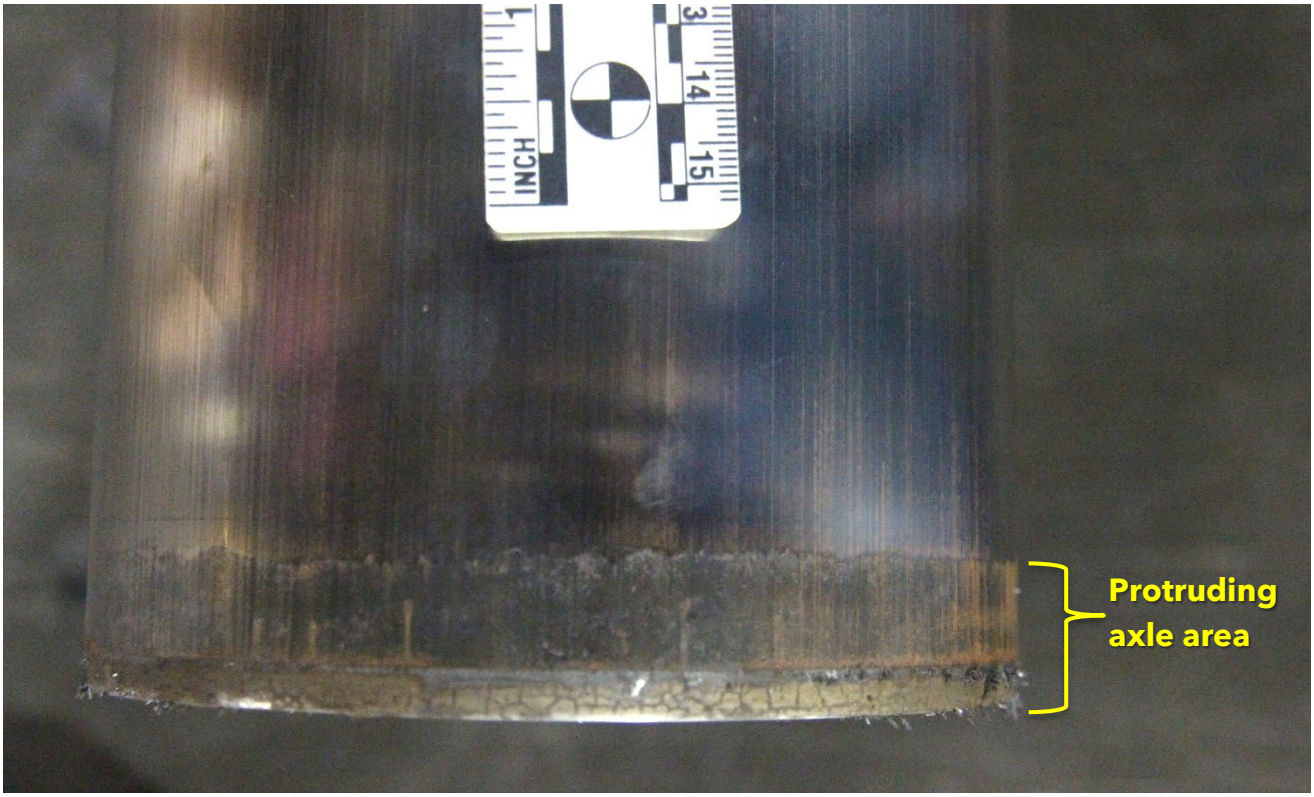

Figure 11. View of the edge of the mating axle seat of the wheel from Figure 10, after disassembly.

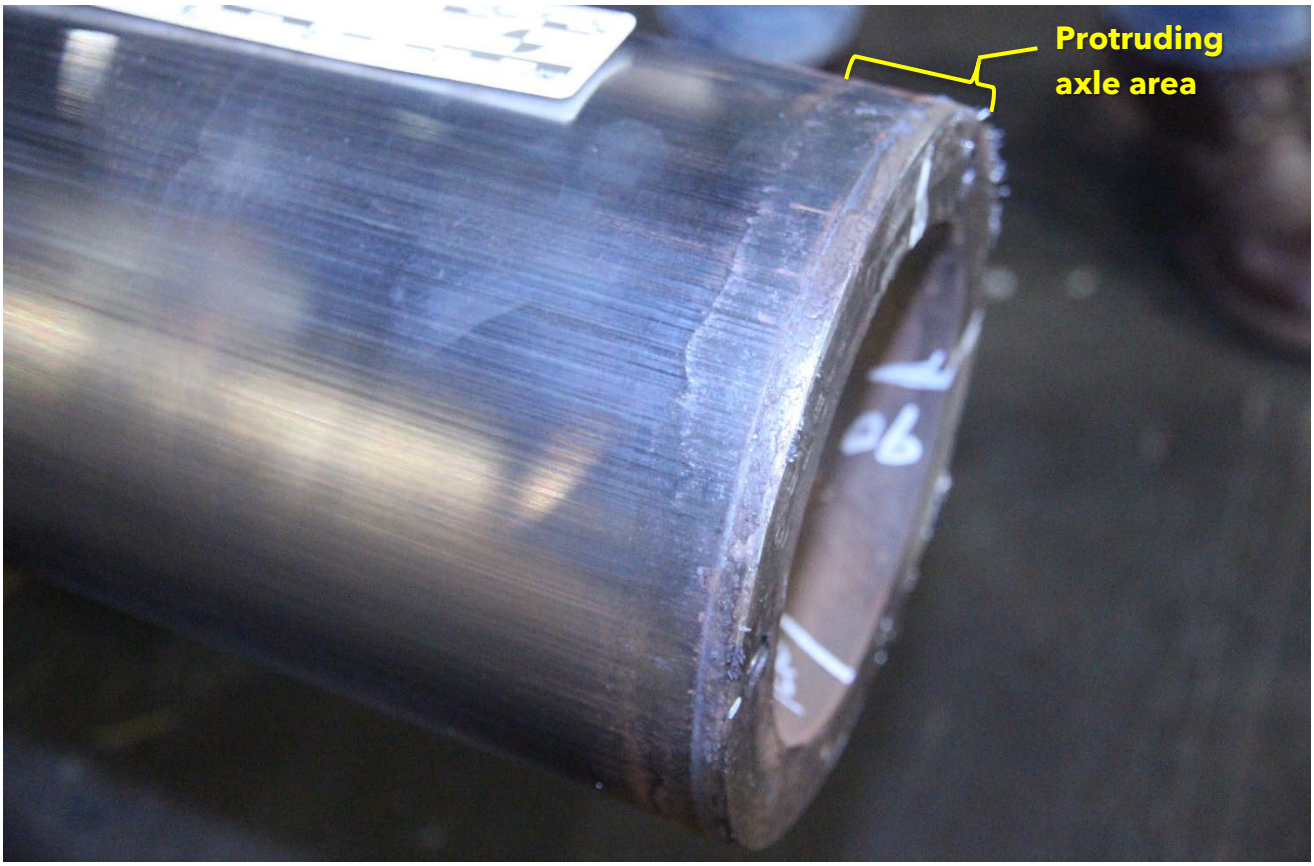

Figure 12. Angled view of the axle wheel seat from Figure 11.

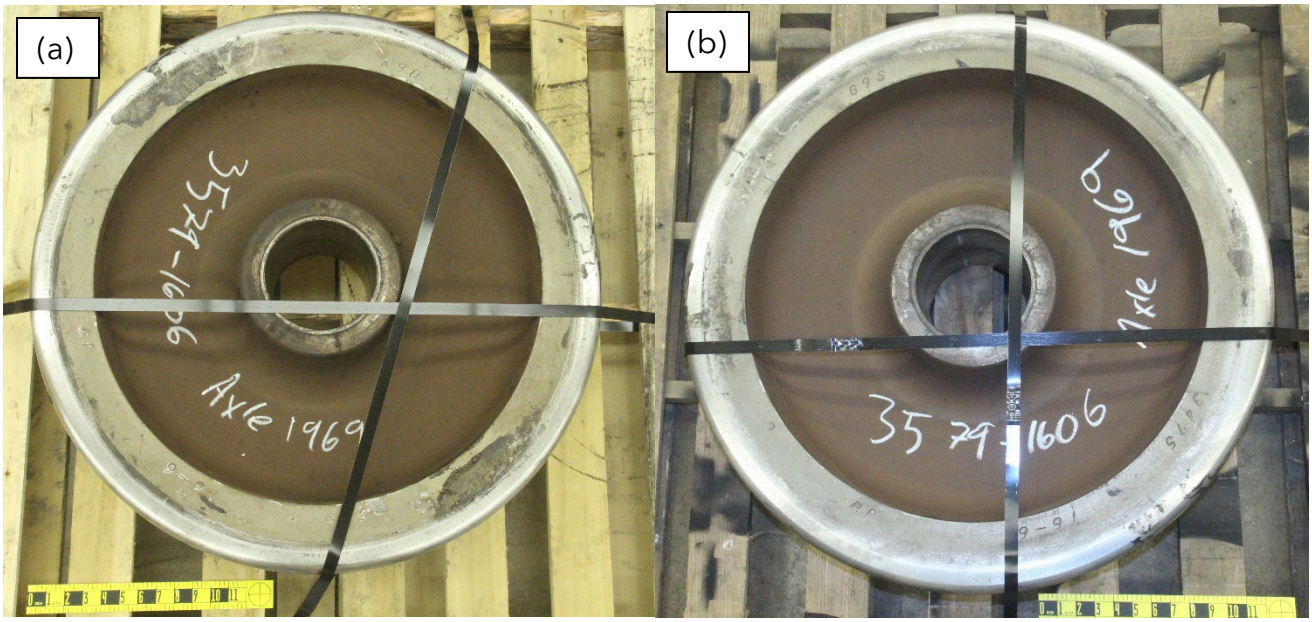

Figure 13. View of the (a) RS and (b) LS wheels from axle 1969, as received viewed from the inboard faces.

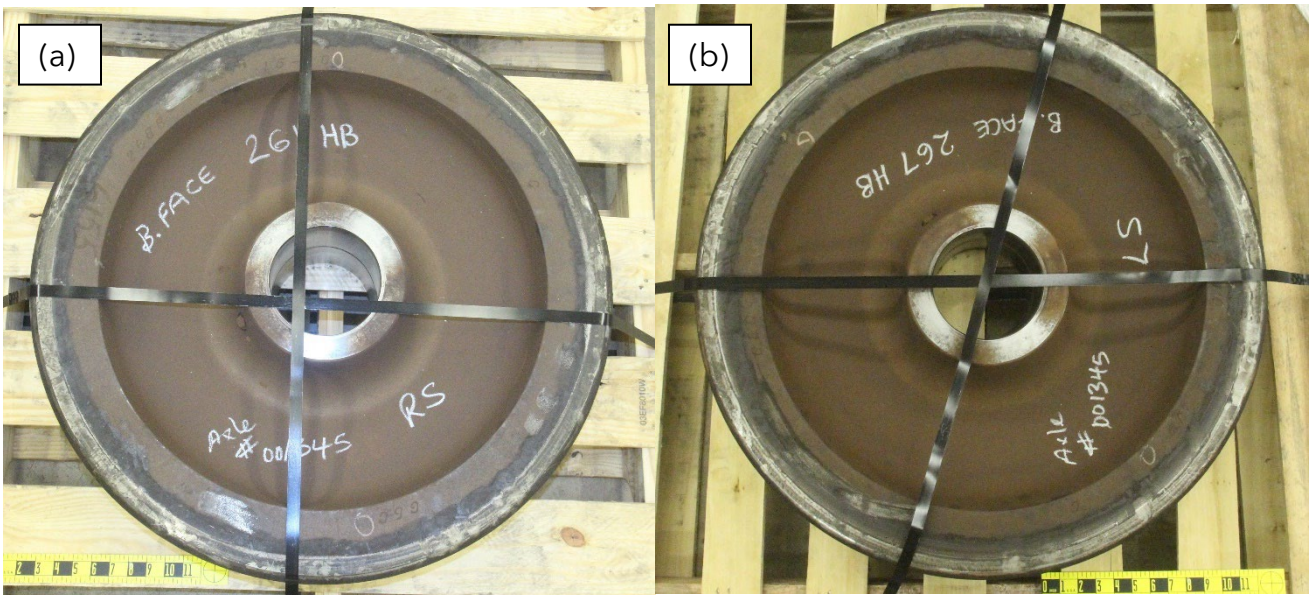

Figure 14. View of the (a) RS and (b) LS wheels from axle 1345, as received viewed from the inboard faces.

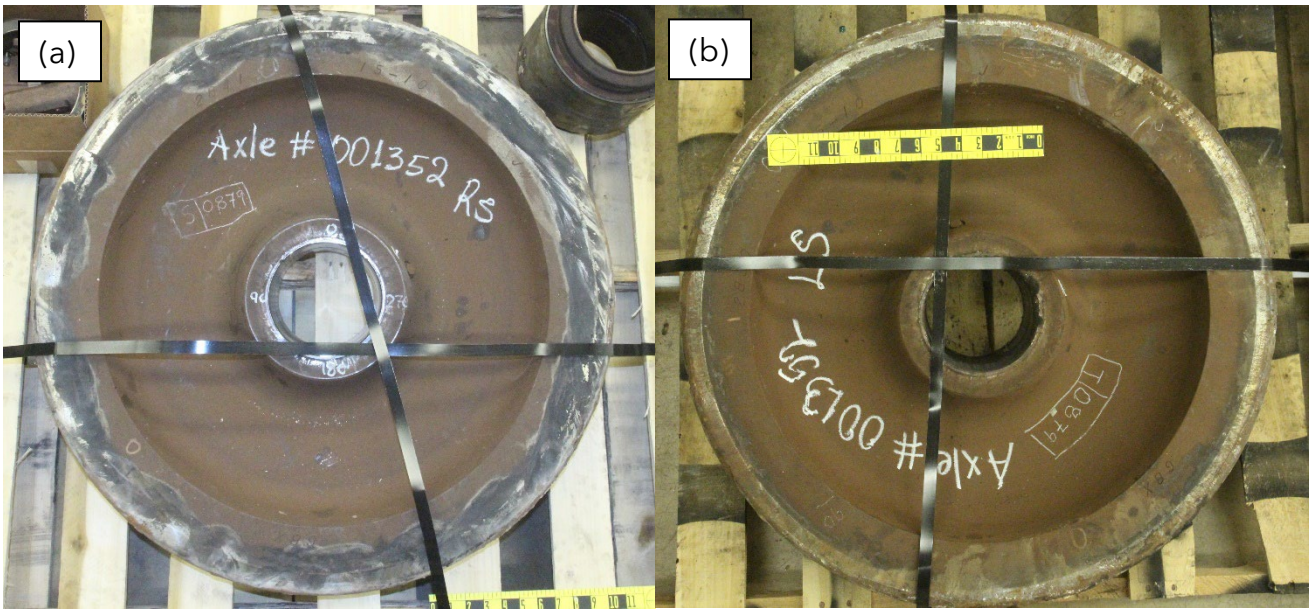

Figure 15. View of the (a) RS and (b) LS wheels from axle 1352, as received viewed from the inboard faces.

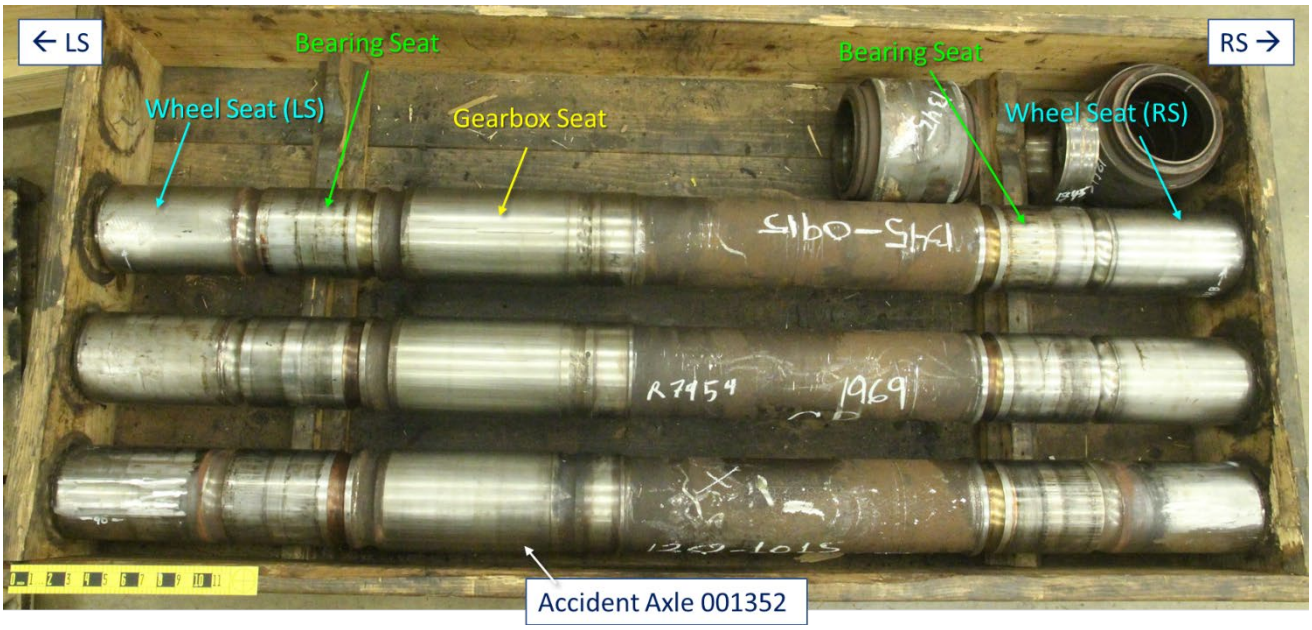

Figure 16. View of the three axles, as received, with the accident axle 001352, on the bottom.

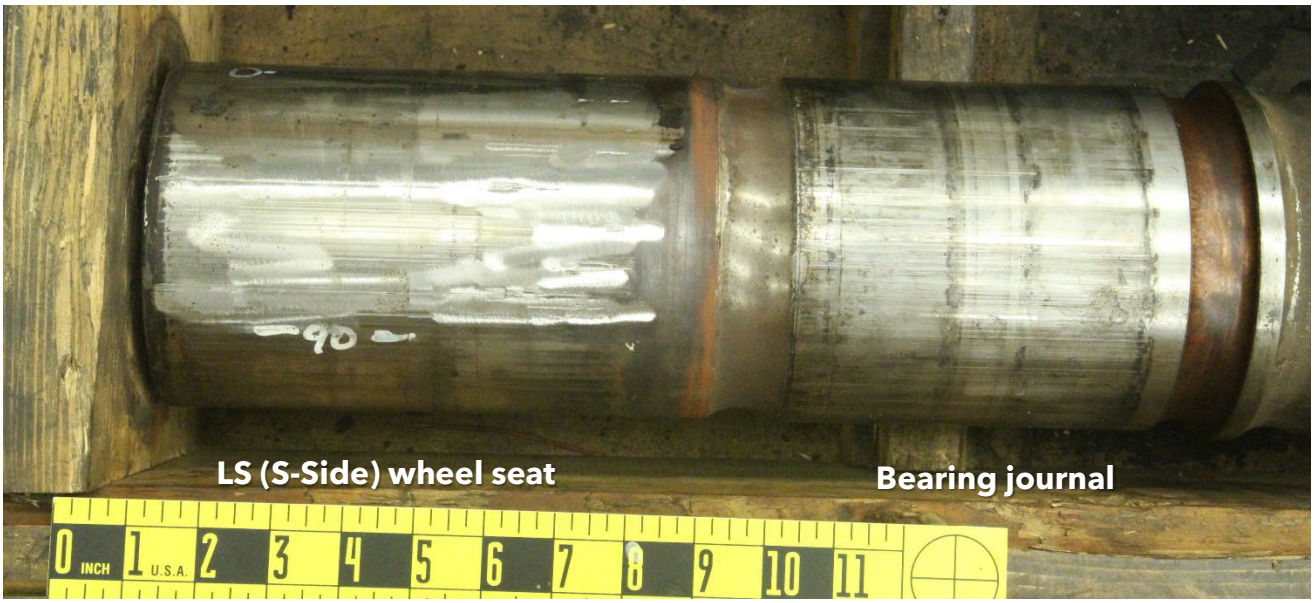

Figure 17. The left side wheel seat and bearing journal from the accident axle, 1352, as received.

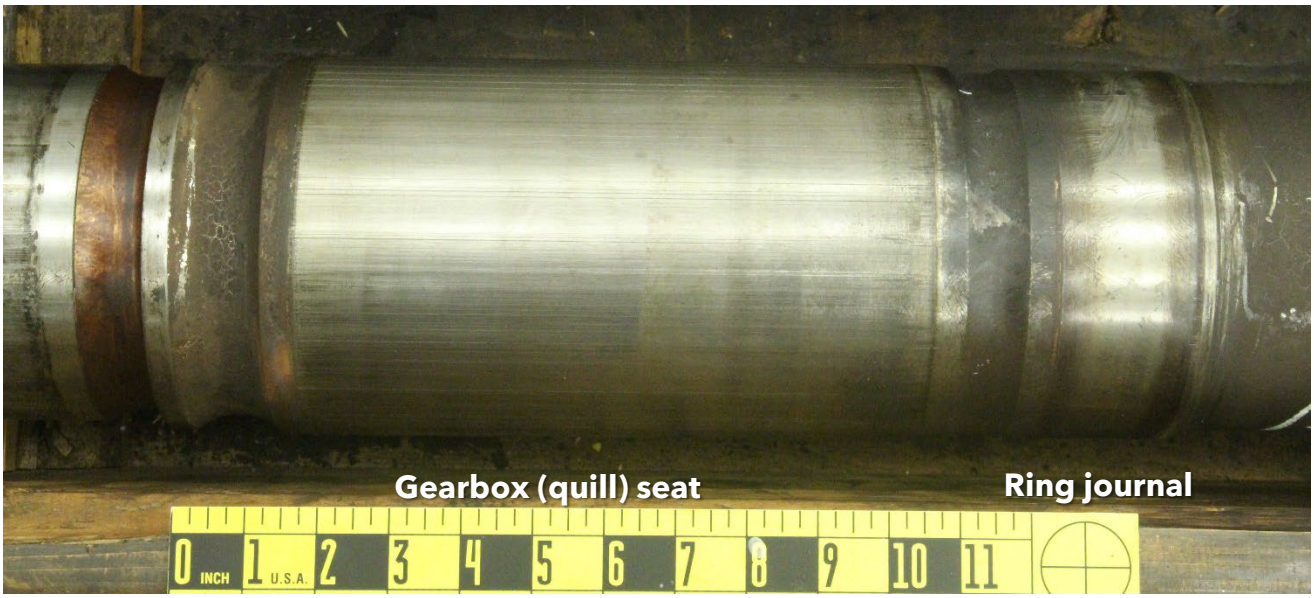

Figure 18. The seat of the gearbox from the accident axle, as received.

Figure 19. The right side bearing journal and wheel seat of the accident axle, as received.

Figure 20. The right side wheel seat on the accident axle, as received.

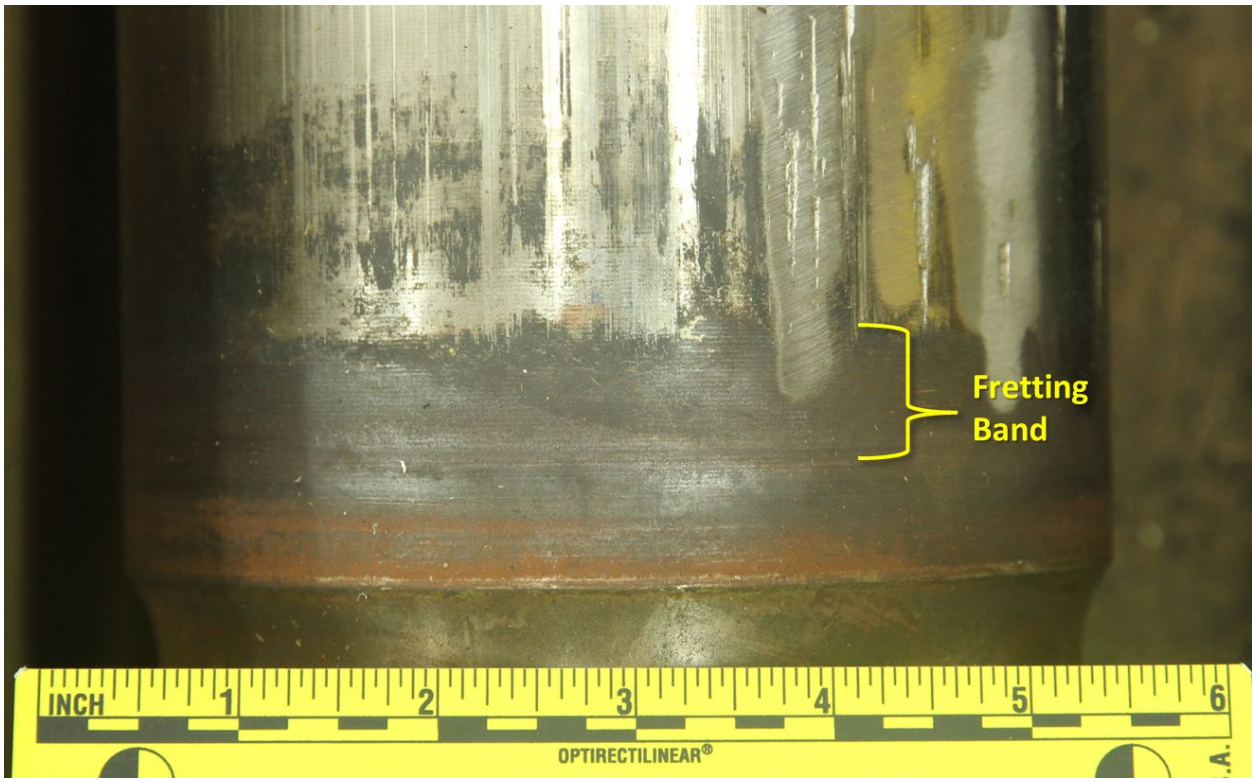

Figure 21. View of the inside end of the LS axle wheel seat, as received, showing the location of the fretting band, identified Figure 22.

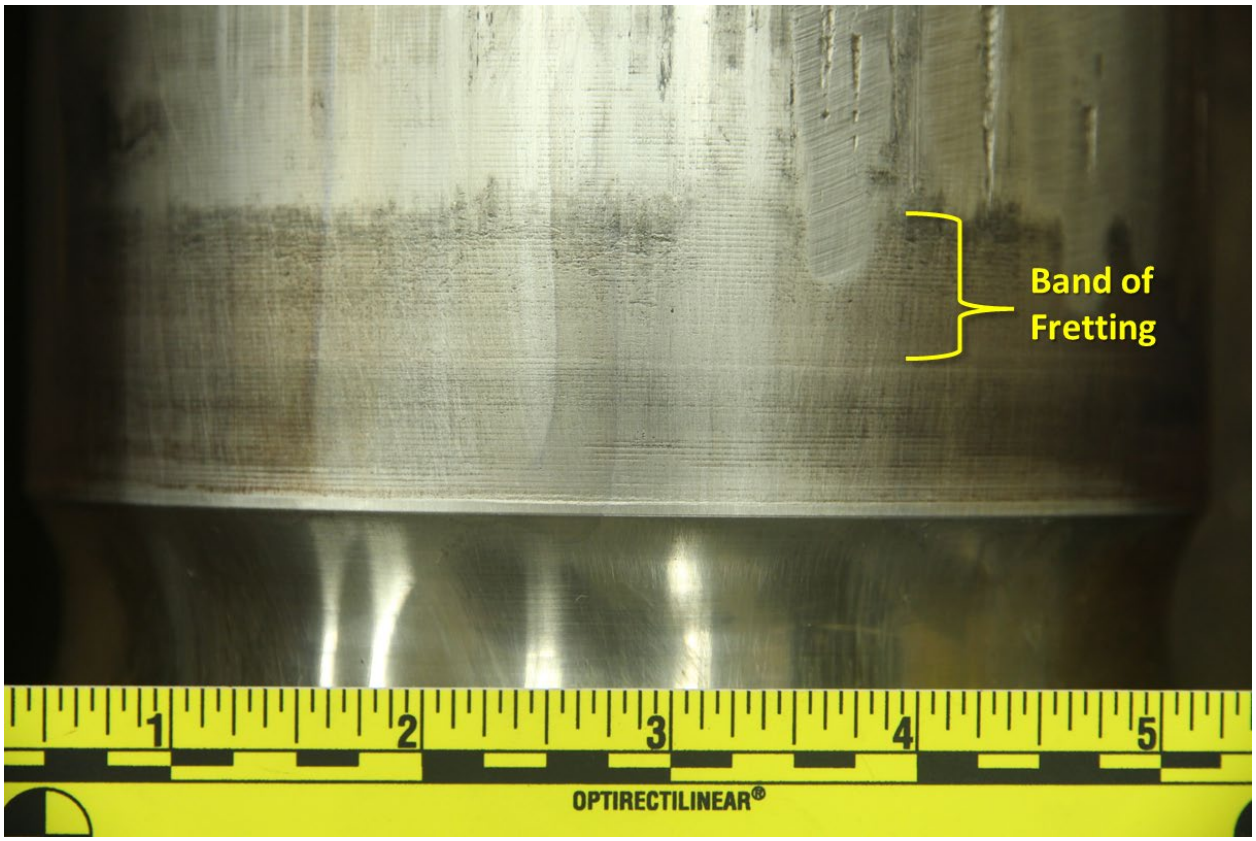

Figure 22. Location of the fretting band in the inboard LS axle wheel seat.

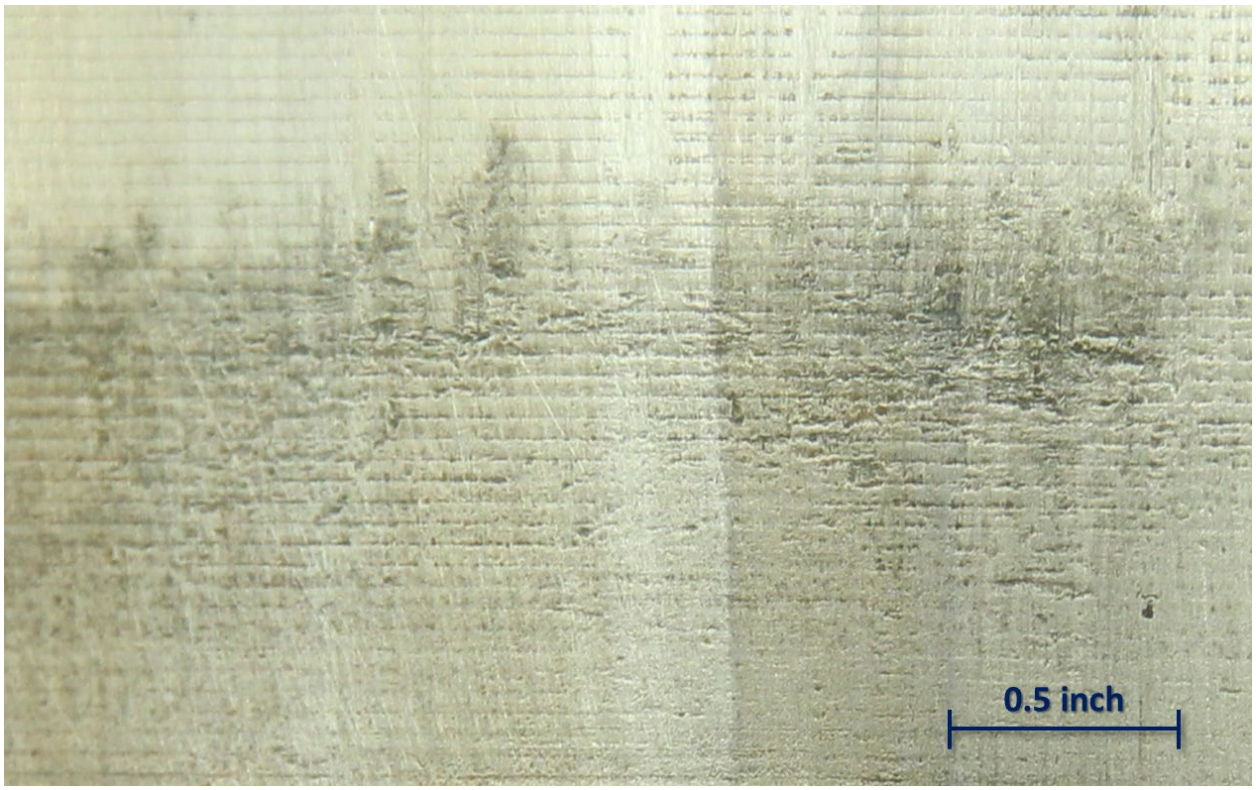

Figure 23. Closer view of fretting damage on the inboard area of the LS wheel seat.

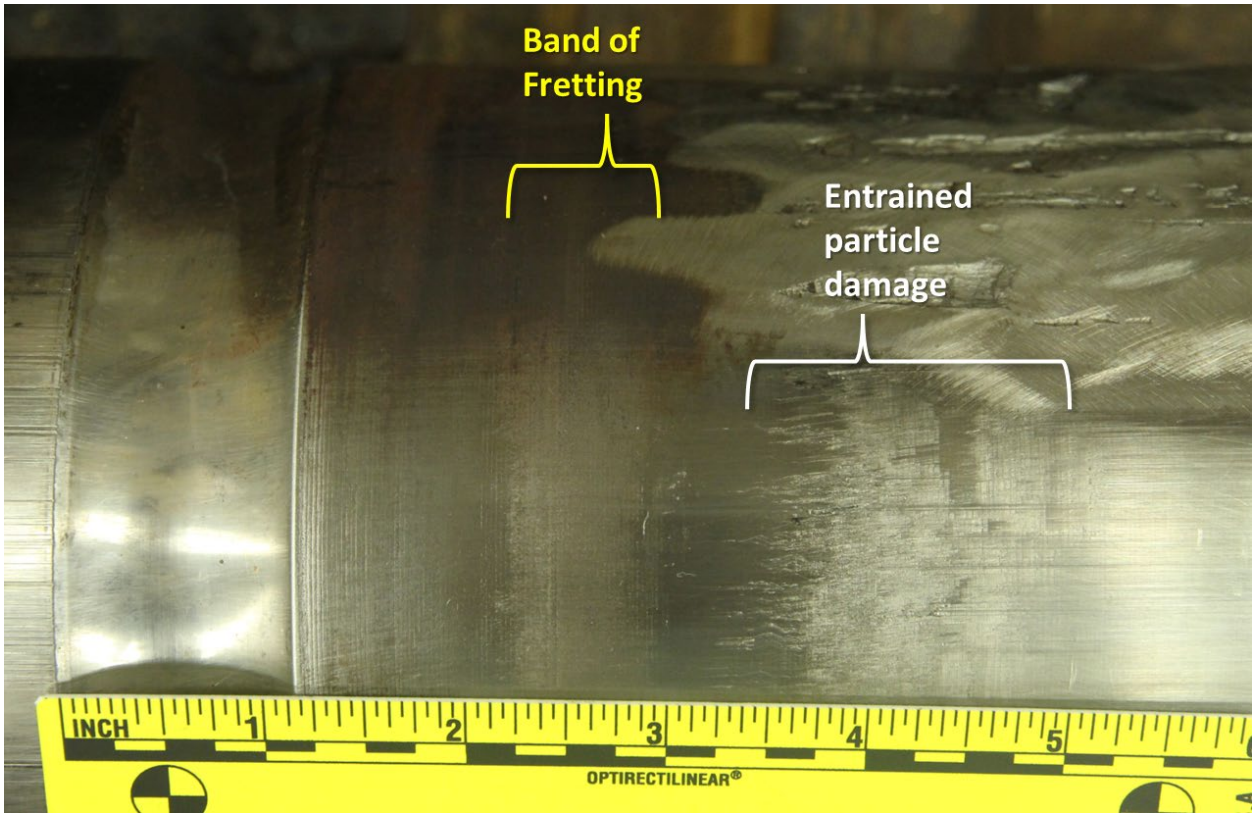

Figure 24. View of the inboard portion of the RS wheel seat after partial cleaning, showing a band of fretting, and areas of entrained particle damage outboard.

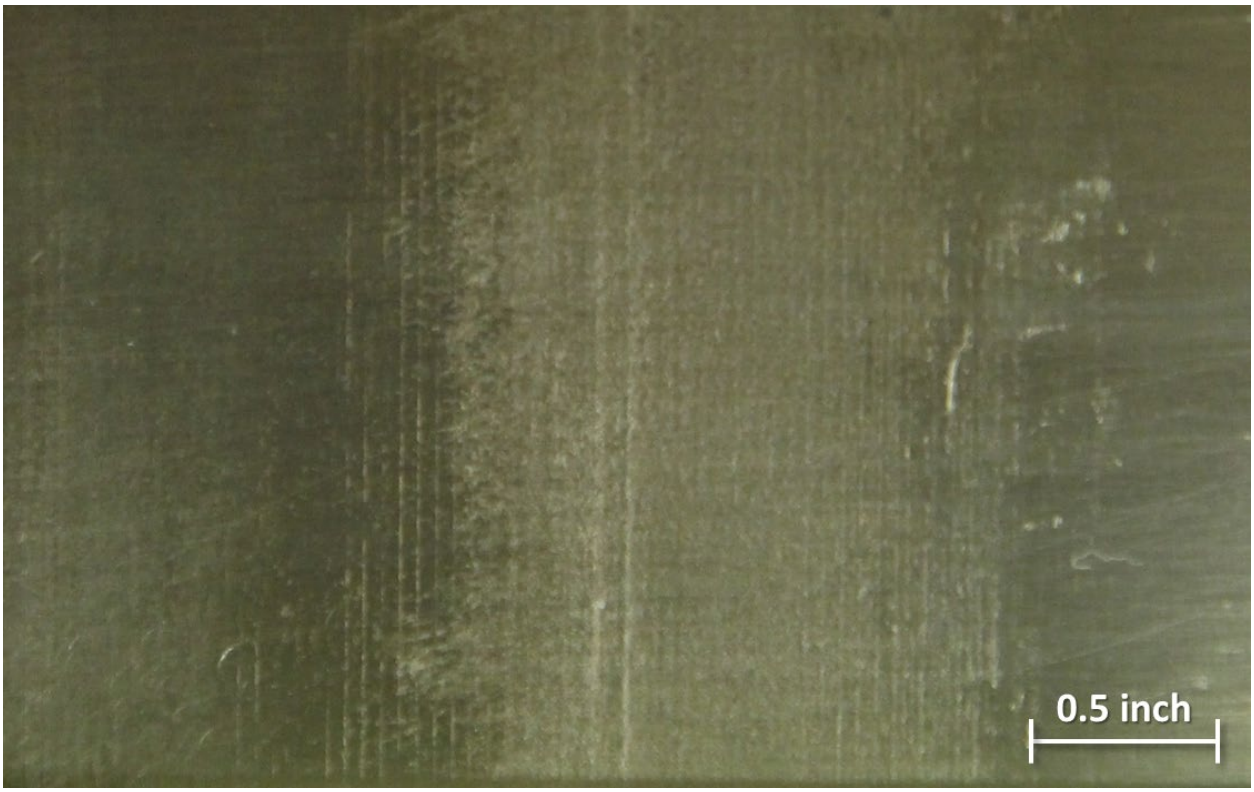

Figure 25. Closer view of the fretting damage on the RS wheel seat.

Figure 26. View of the gearbox assembly from the accident wheelset.

Figure 27. View of the left side brake disc, as received.

Figure 28. View of the fracture surface from the left side brake disc, as received.

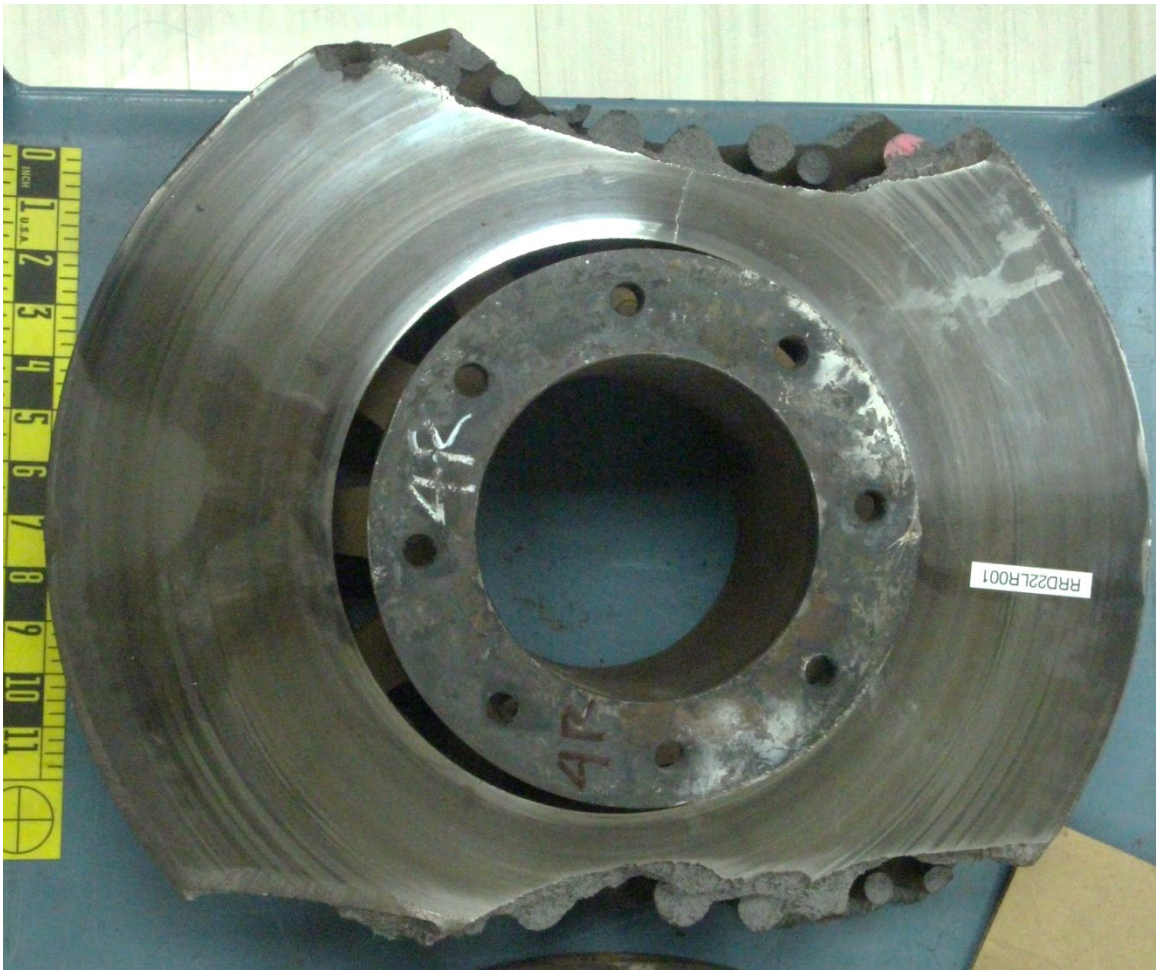

Figure 29. View of the opposite or right side brake disc, as received.

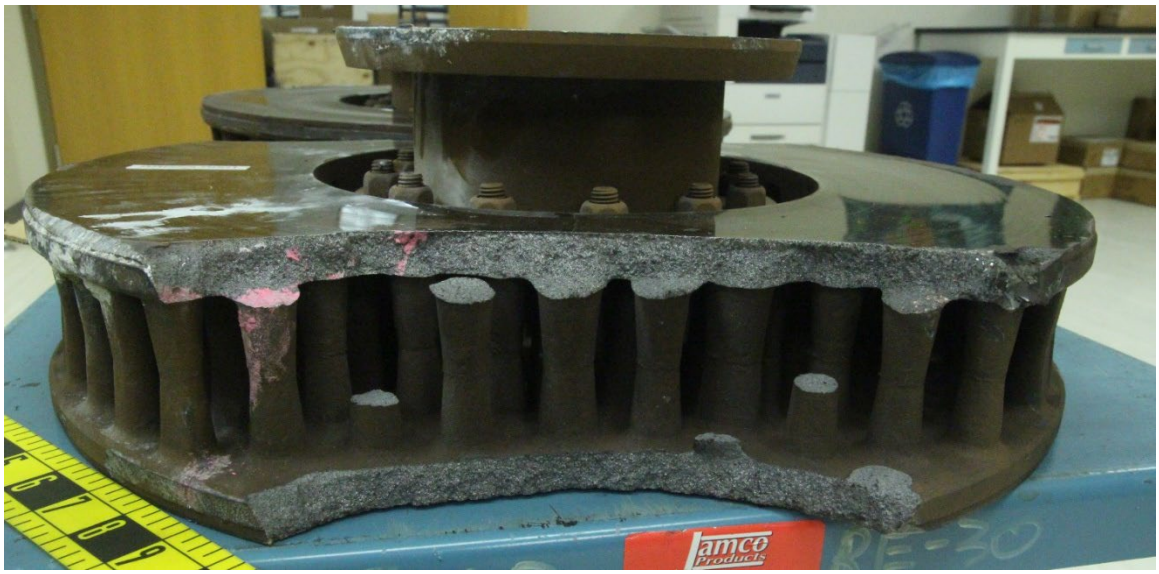

Figure 30. View of the fracture surface of the right side disc surface in Figure 29.

Figure 31. Opposite views of the brake disc remnants that mates with the right side fracture surface in Figure 30.

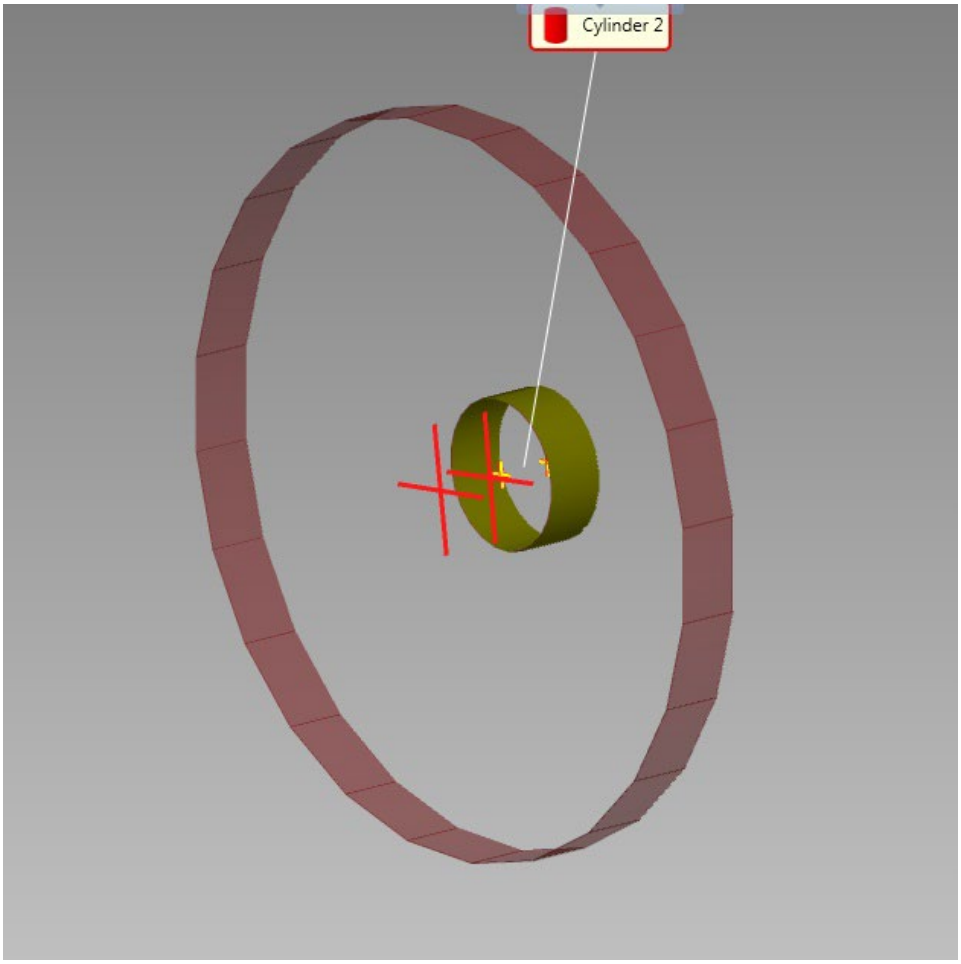

Figure 32. Wireframe representation of the cylindricity and concentricity of the accident wheel measurements.

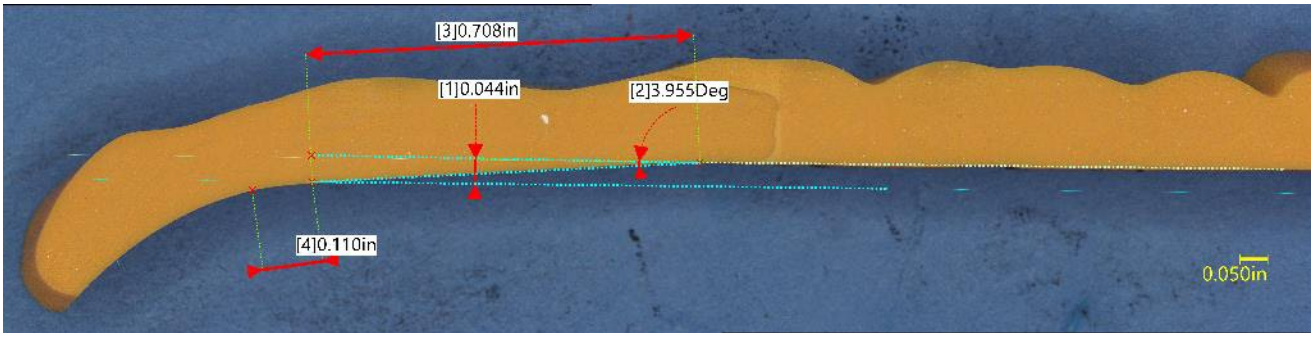

Figure 33. Cross section of a reproduction rubber negative an area of the right side wheel, showing various measurements describing the inboard circumferential wear near the flange.

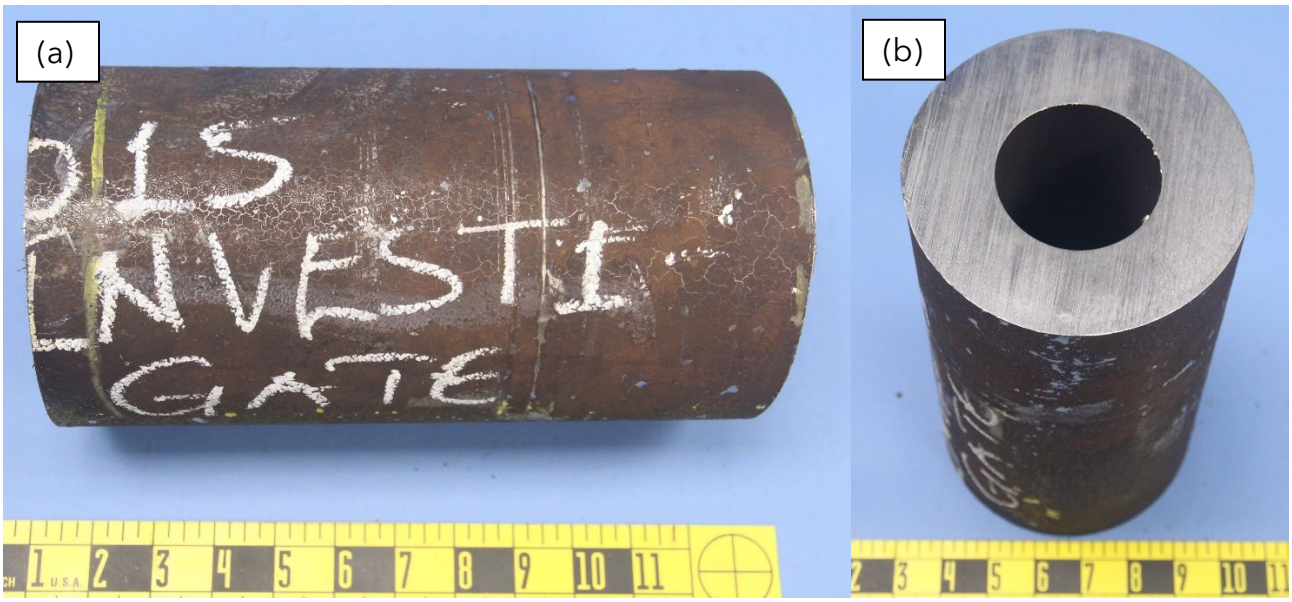

Figure 34. Sections of the accident axle, view from the longitudinal and transverse faces.

Figure 35. Sections of the left side accident wheel.

Figure 36. Cross section view of the left side wheel.

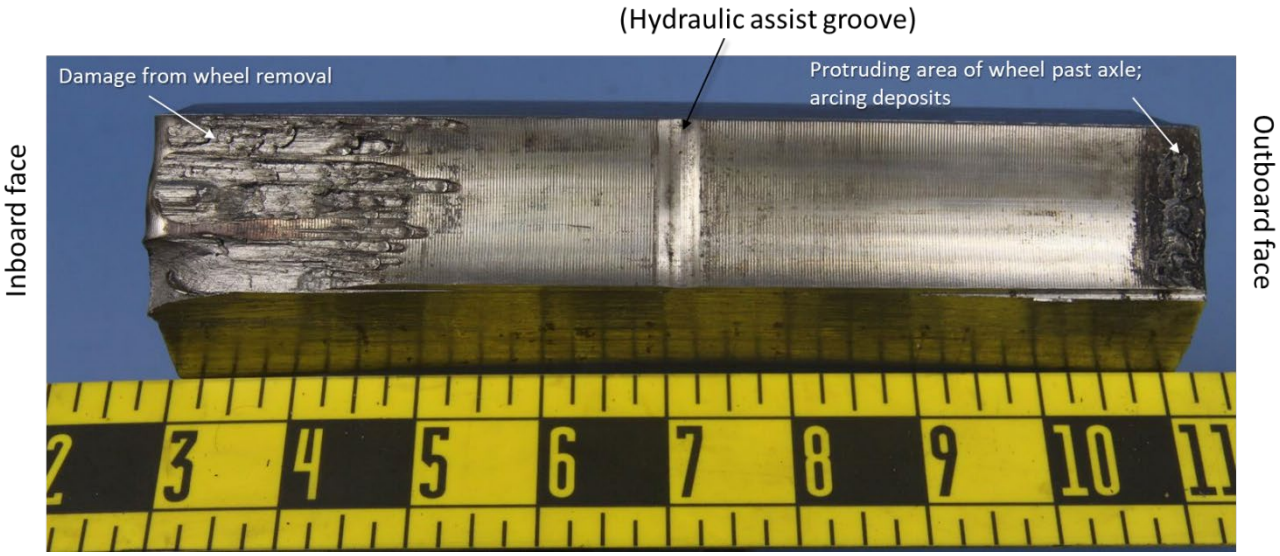

Figure 37. Views of the sectioned left wheel bore, showing damage on the inboard and outboard edges.

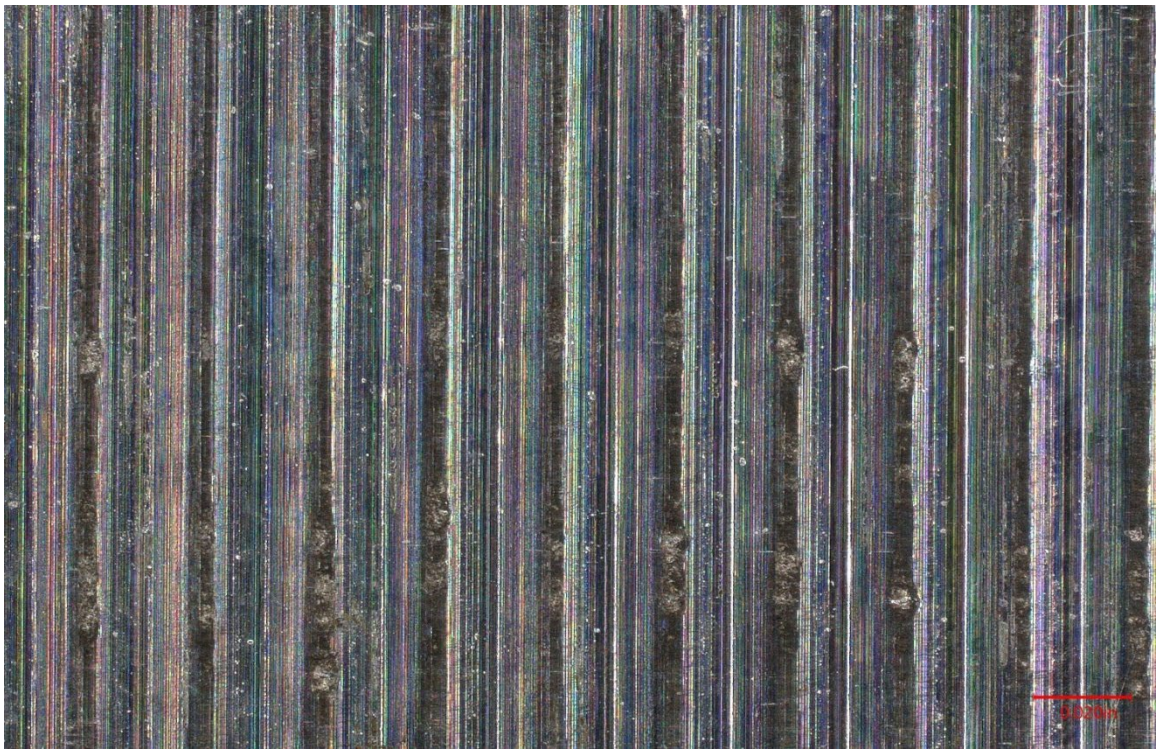

Figure 38. View of the machine marks on the wheel bore surface, taken in an relatively undamaged area.

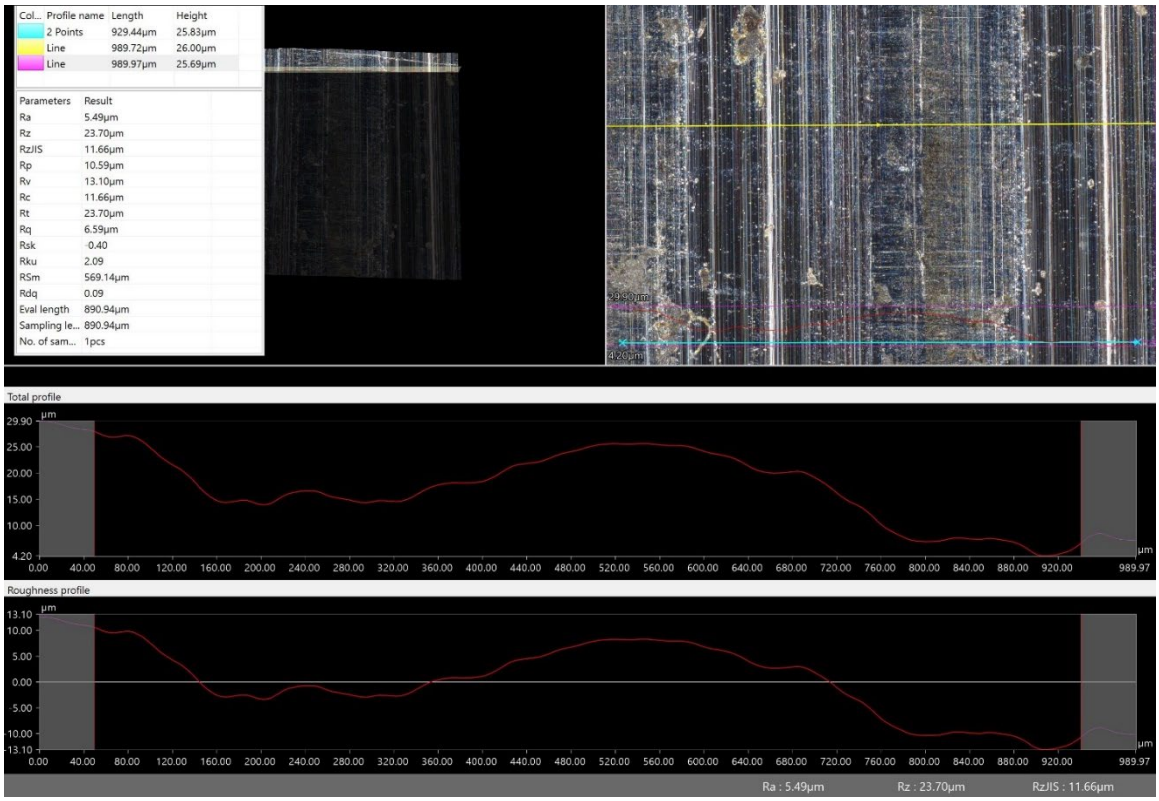

Figure 39. Screen capture of a typical optical roughness measurement of the wheel bore (~200X).

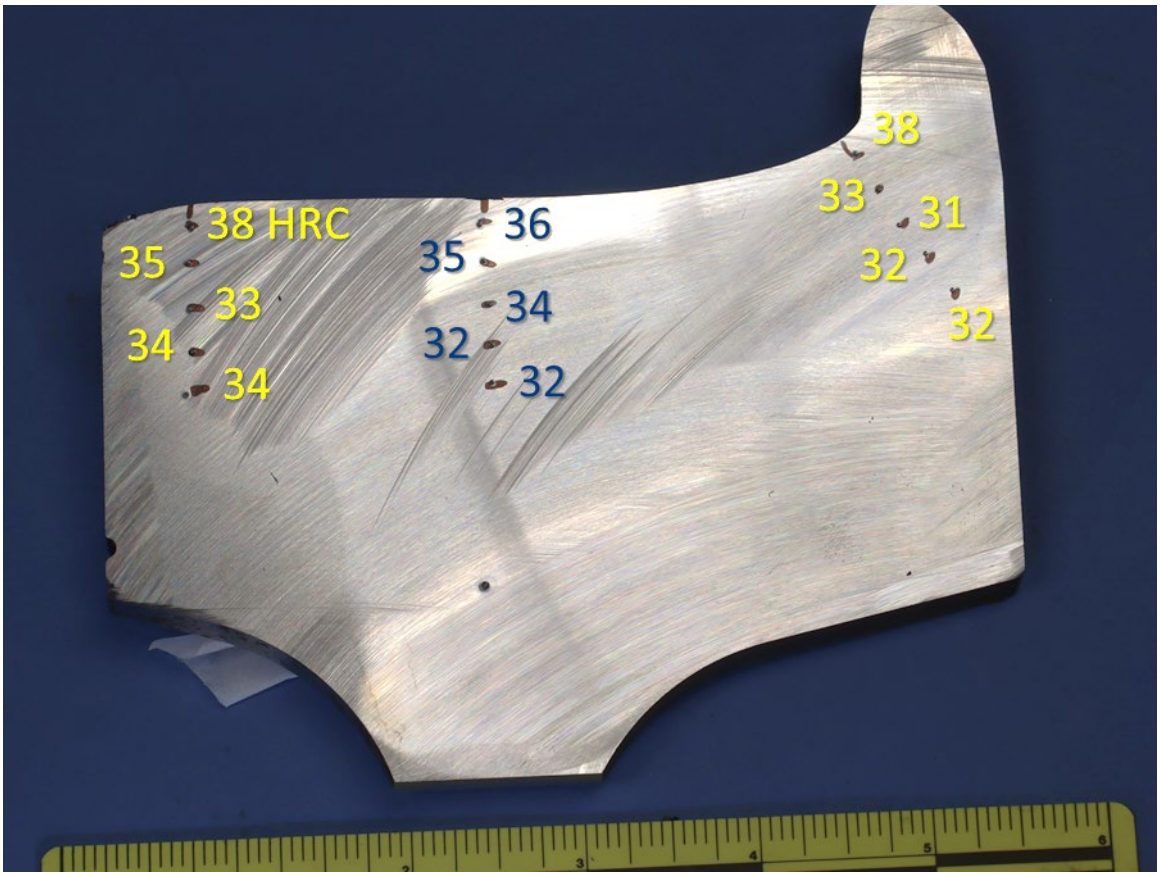

Figure 40. Cross section of the LS wheel, showing the Rockwell hardness indents annotated to show the results.

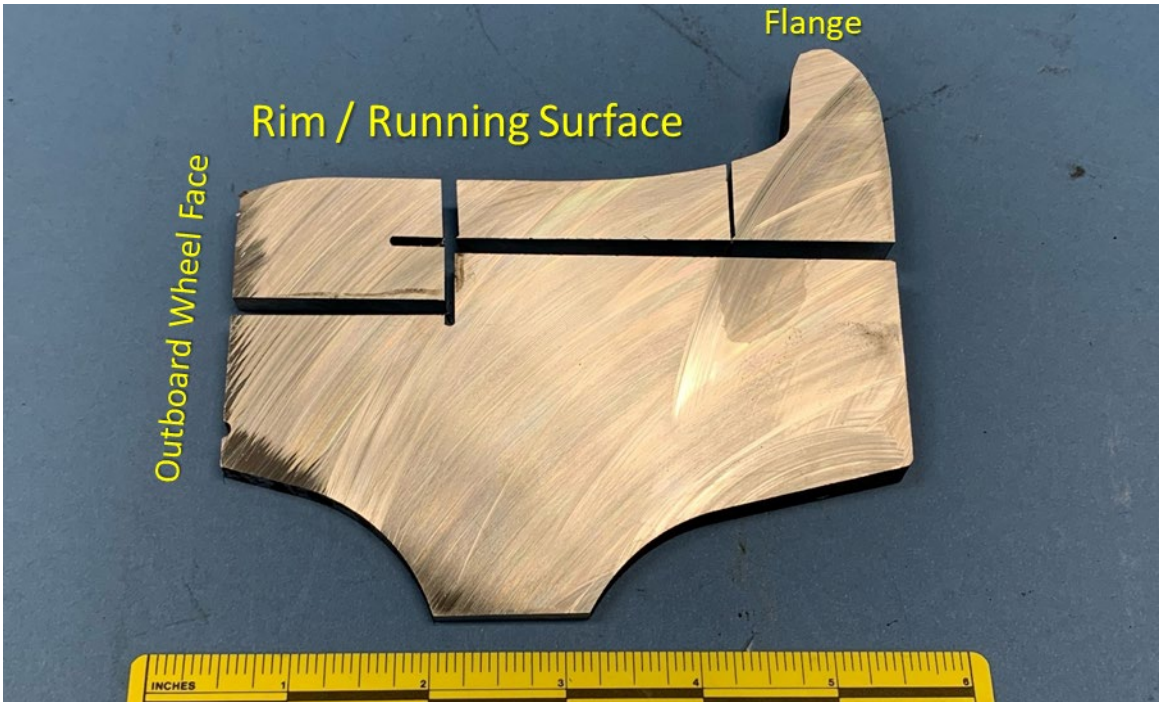

Figure 41. Sections of an adjacent LS wheel cross section from Figure 40.

Figure 42. View of the sectioned fractured piece of the flange.

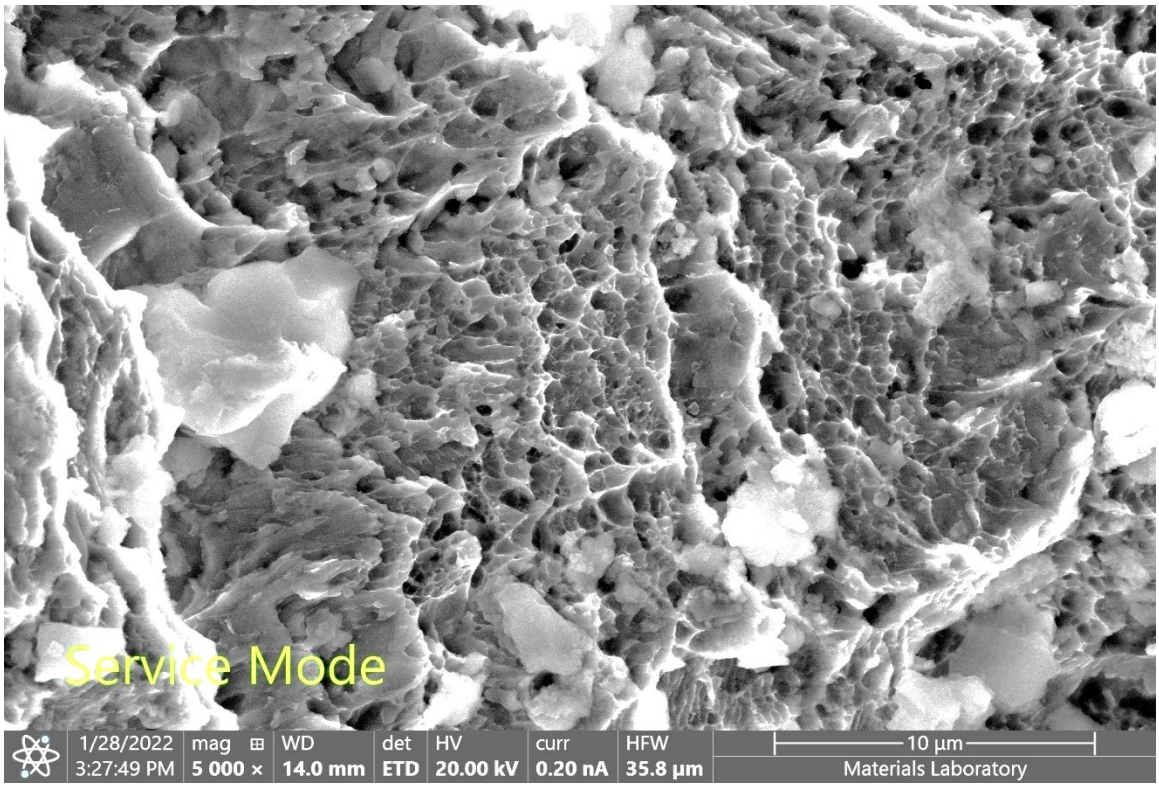

Figure 43. Secondary electron (SE) micrograph of a typical area of the flange fracture surface.

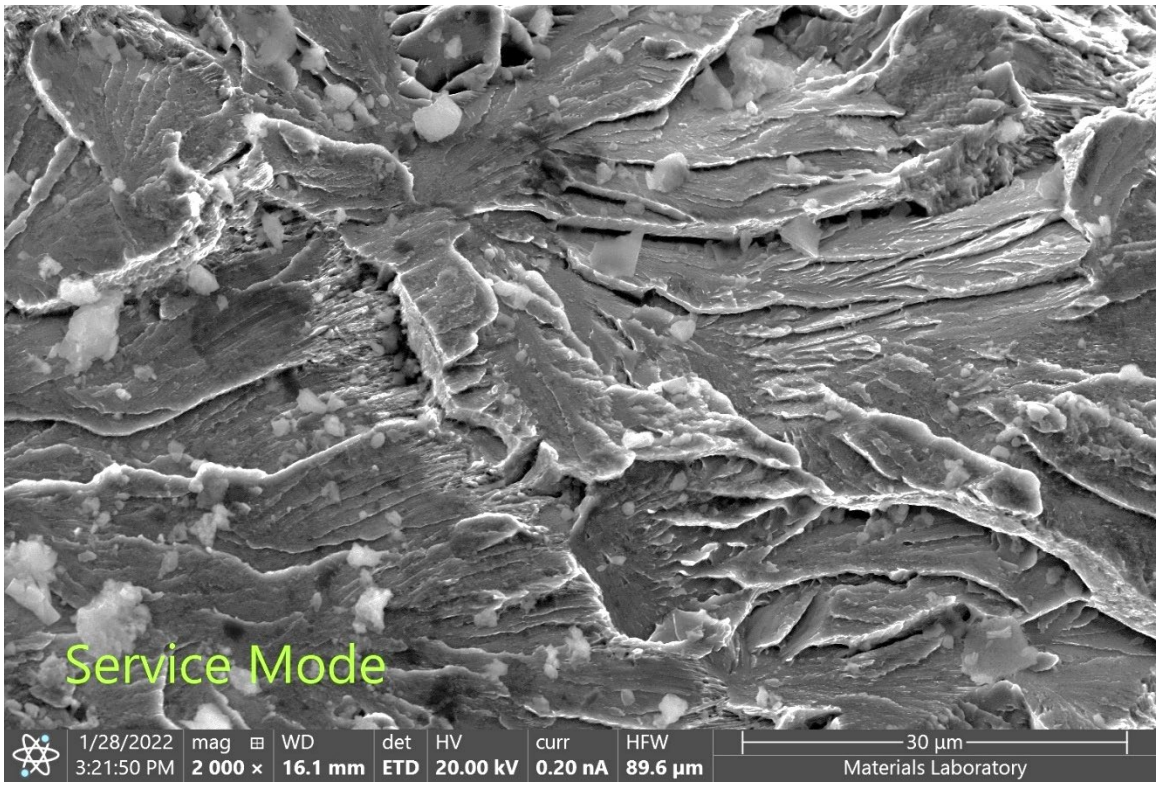

Figure 44. SE micrograph of cleavage facets on the flange fracture.

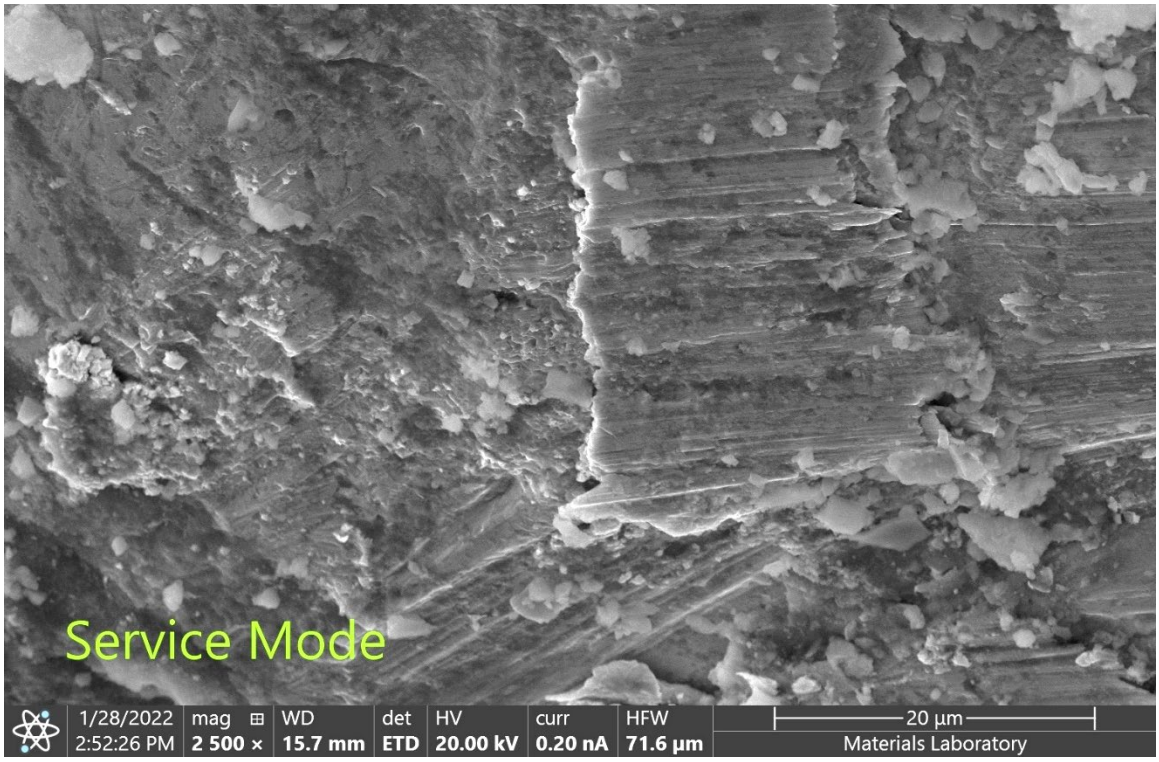

Figure 45. SE micrograph of dimpled rupture and smearing on the flange fracture.

Figure 46. View of the remnant that separated from the RS wheel bore.

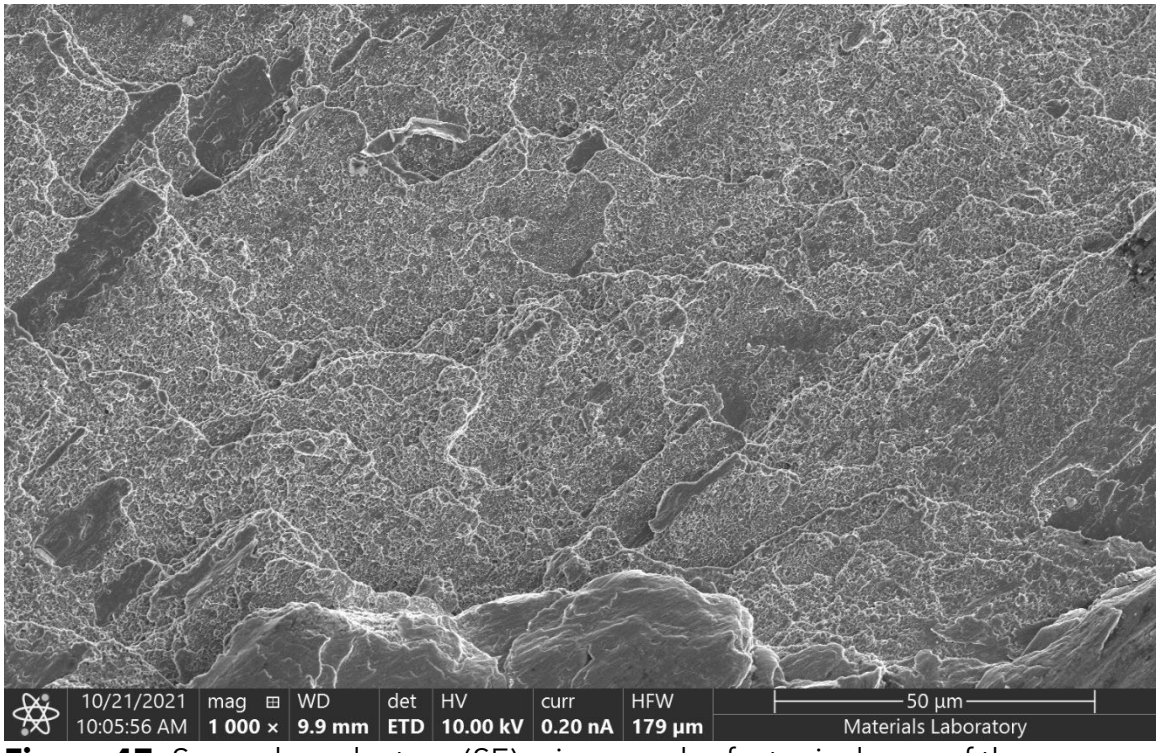

Figure 47. Secondary electron (SE) micrograph of a typical area of the remnant fracture in Figure 46.

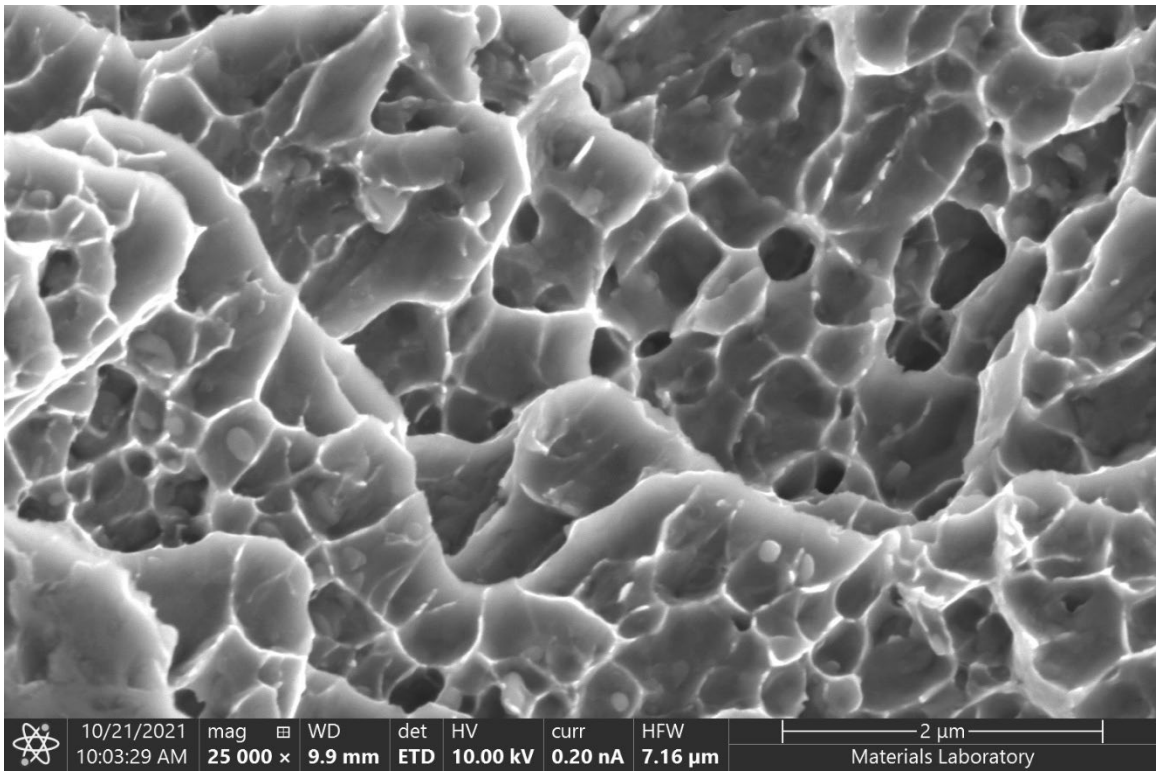

Figure 48. SE micrograph of dimpled rupture on the wheel remnant.

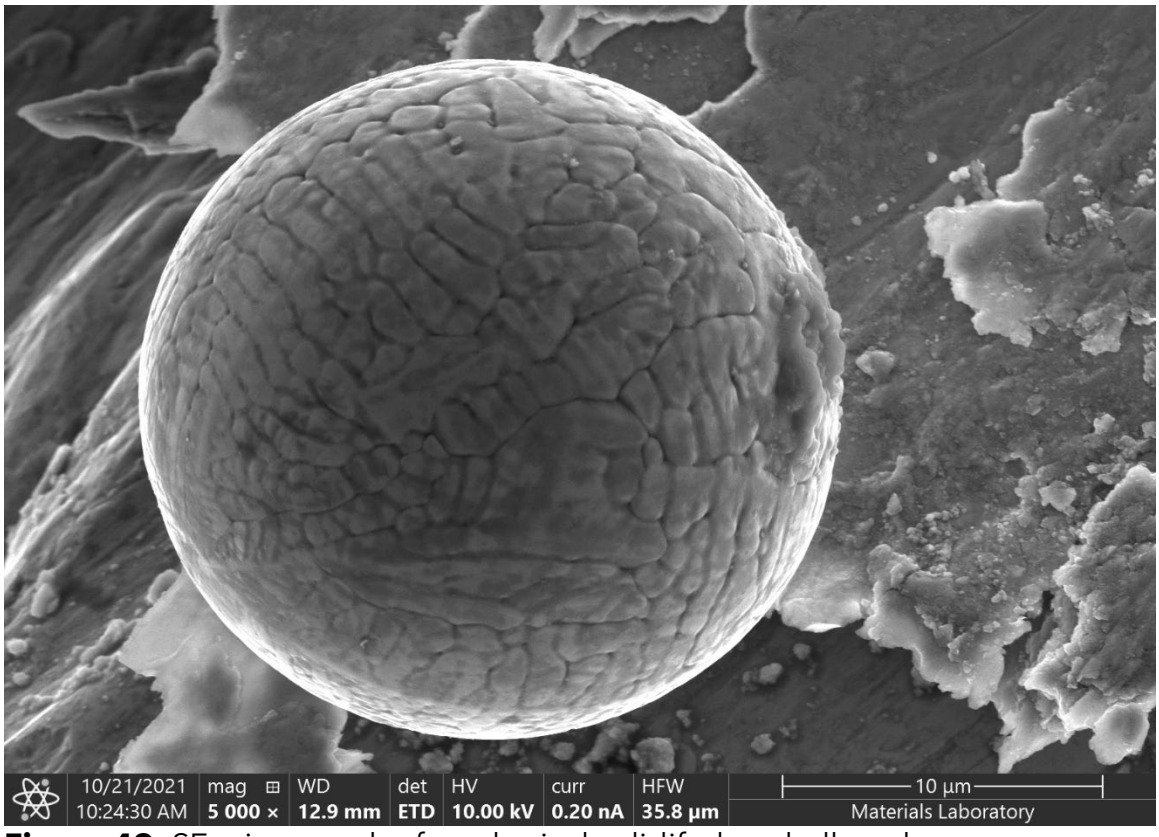

Figure 49. SE micrograph of a spherical solidifed arc ball on the remnant.

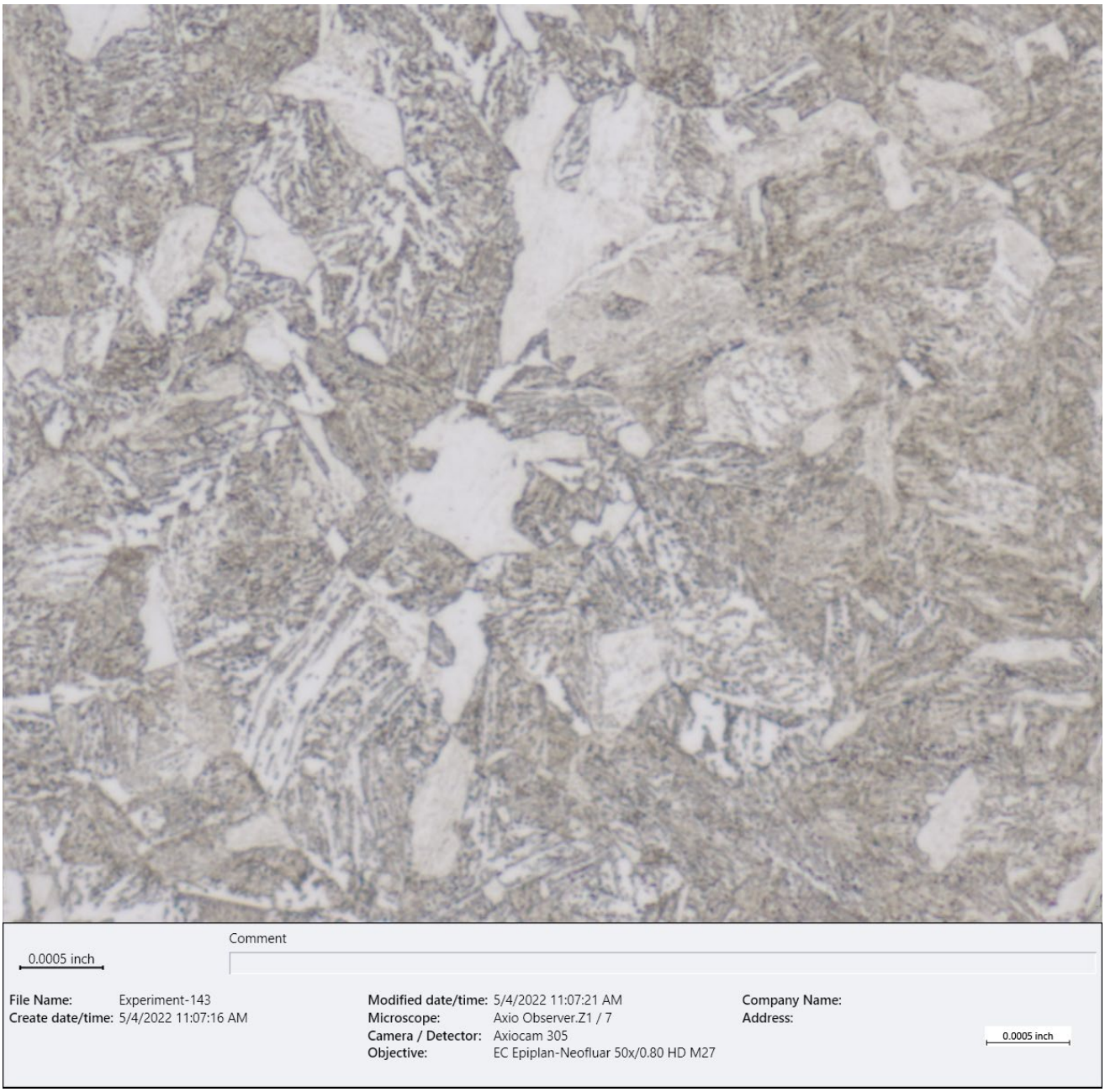

Figure 50. Bright field (BF) optical micrograph of a typical view of the accident axle microstructure (etched 2% Nital, ~1000X).

Figure 51. BF optical micrographs of a typical area of the LS wheel core microstructure (~500X, etched 2% nital).

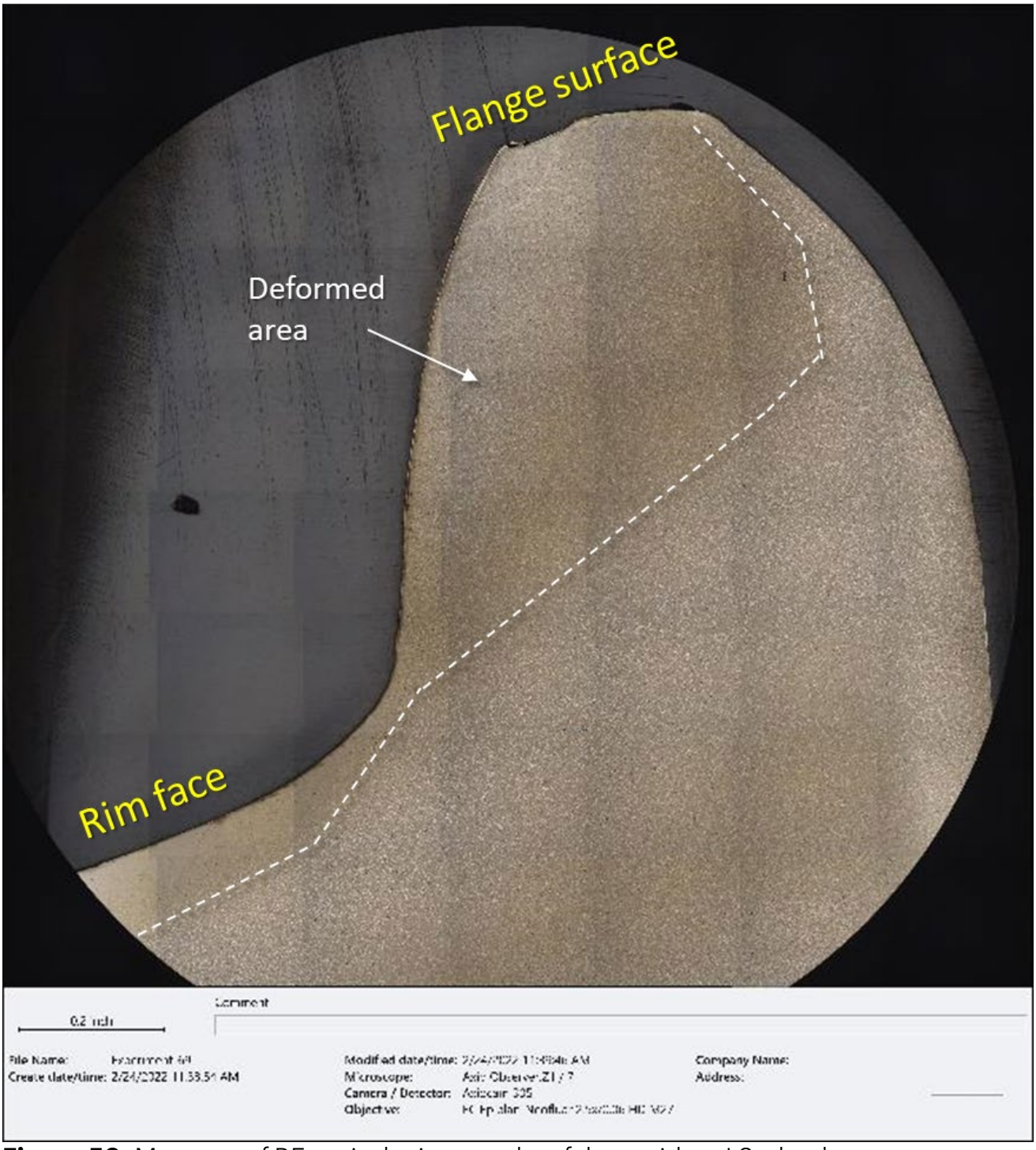

Figure 52. Montage of BF optical micrographs of the accident LS wheel cross section, annotated to show the deformed area of the microstructure on the flange and rim face (etched 2% Nital, ~25X).

Figure 53. BF optical micrograph of the outboard edge of the LS wheel flange, showing deformation and surface martensite (~100X, etched 2% Nital).

Figure 54. BF optical micrograph of the deformed grains and surface martensite of the wheel rim surface (~200X, etched 2% nital).

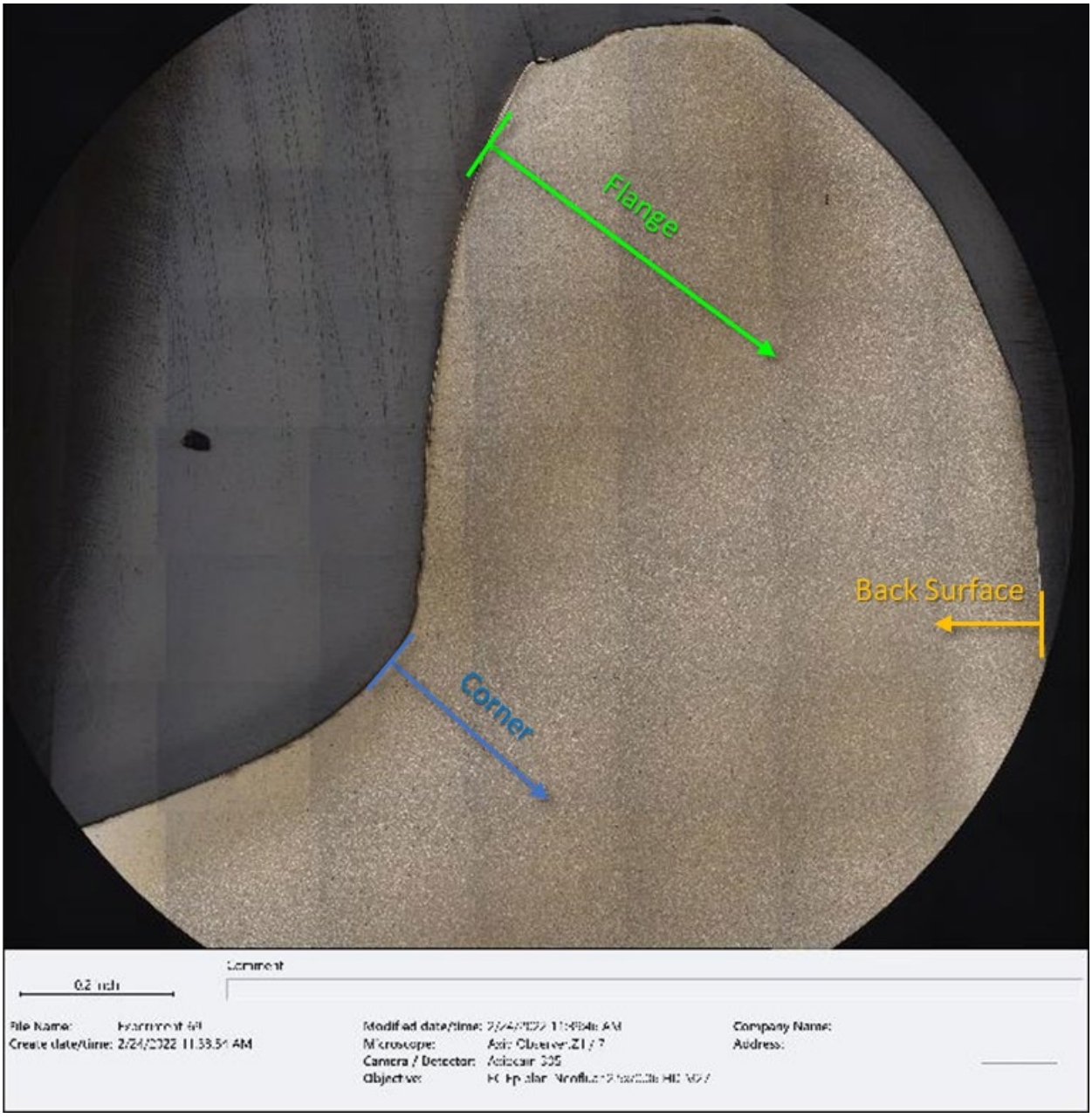

Figure 55. Annotated version of Figure 52, showing the locations of the microindentation hardness paths.

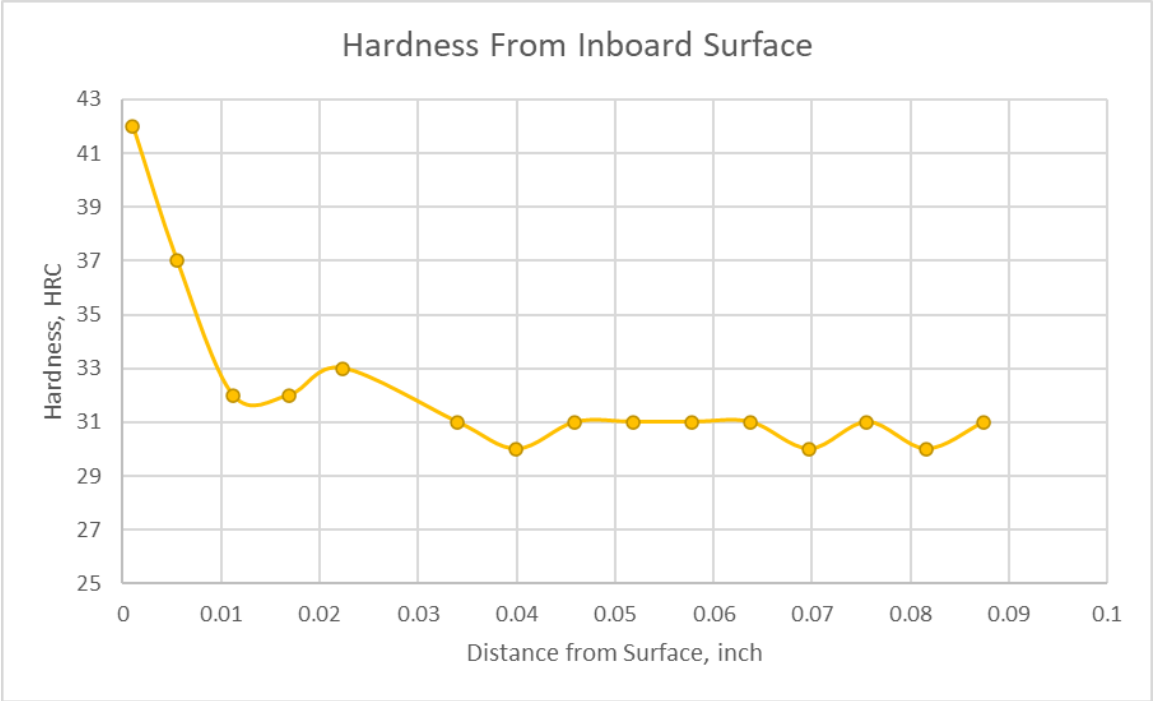

Figure 56. Chart of the hardness on the from the inboard worn surface, in HRC converted from HV_{500}.

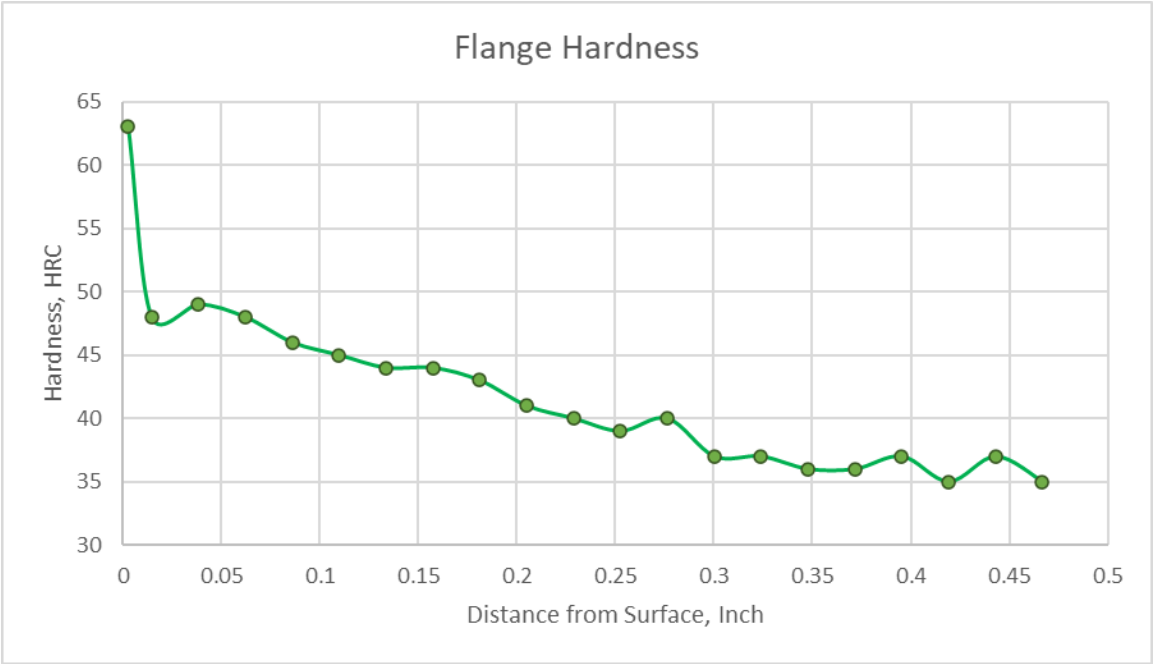

Figure 57. Chart of the hardness on the from the flange surface, in HRC converted from HV_{500}.

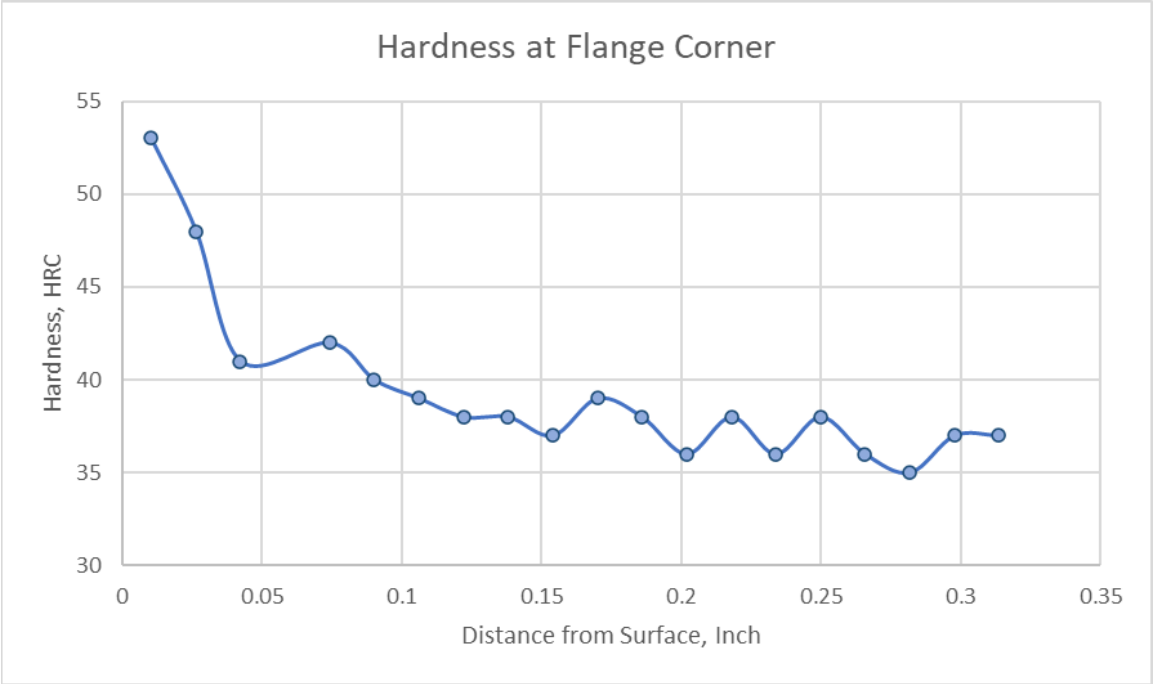

Figure 58. Chart of the hardness on the from the rim corner surface, in HRC converted from HV_{500}.

Figure 59. Montage of BF optical micrographs of the corner of the outboard wheel face and bore (~10X, etched 2% Nital).

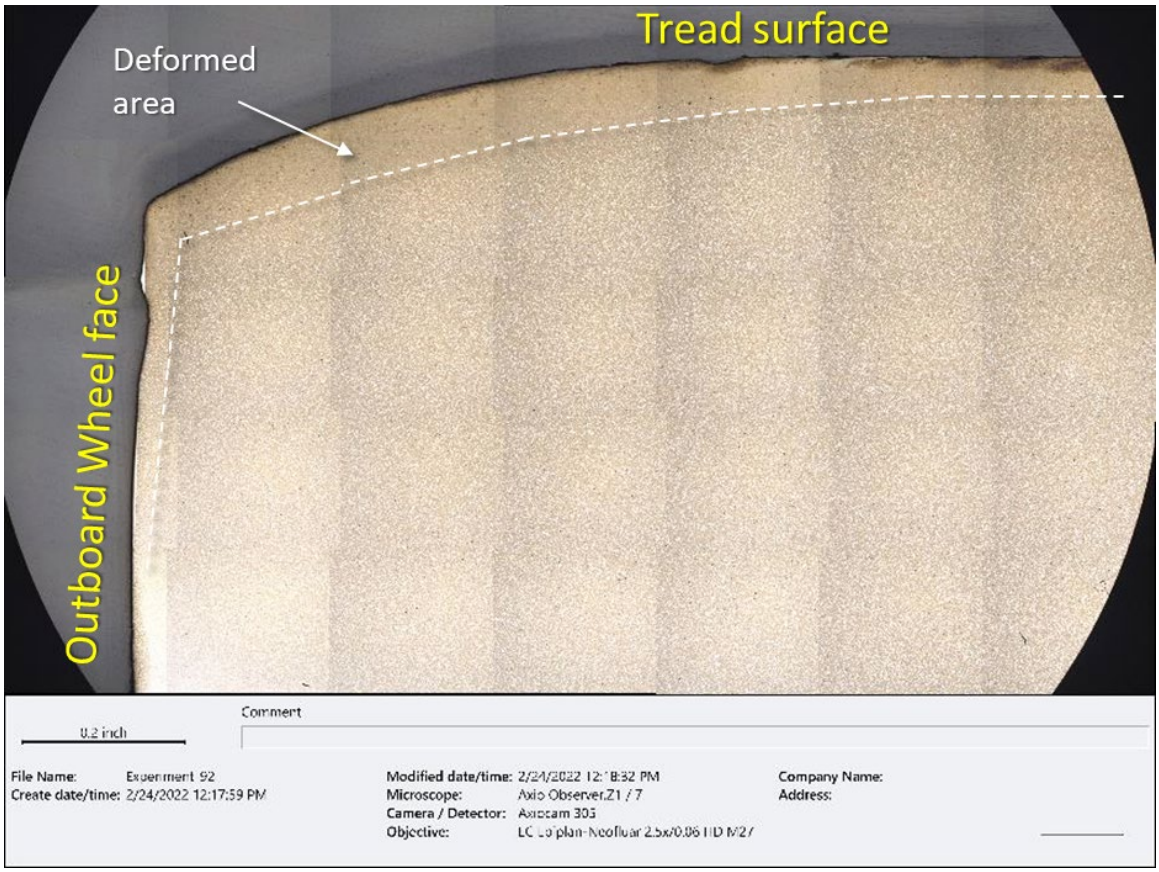

Figure 60. Closer montage view of the corner in Figure 59, showing the deformated area (~25X, etched 2% Nital).

Figure 61. Closer view of the outboard face of the LS wheel microstructure, showing a jump, lumpy layer (~200X, etched 2% Nital).

Figure 62. BF optical micrograph of outboard face in Figure 61, showing deformed grains and a surface martensite layer (~500X, etched 2% nital).

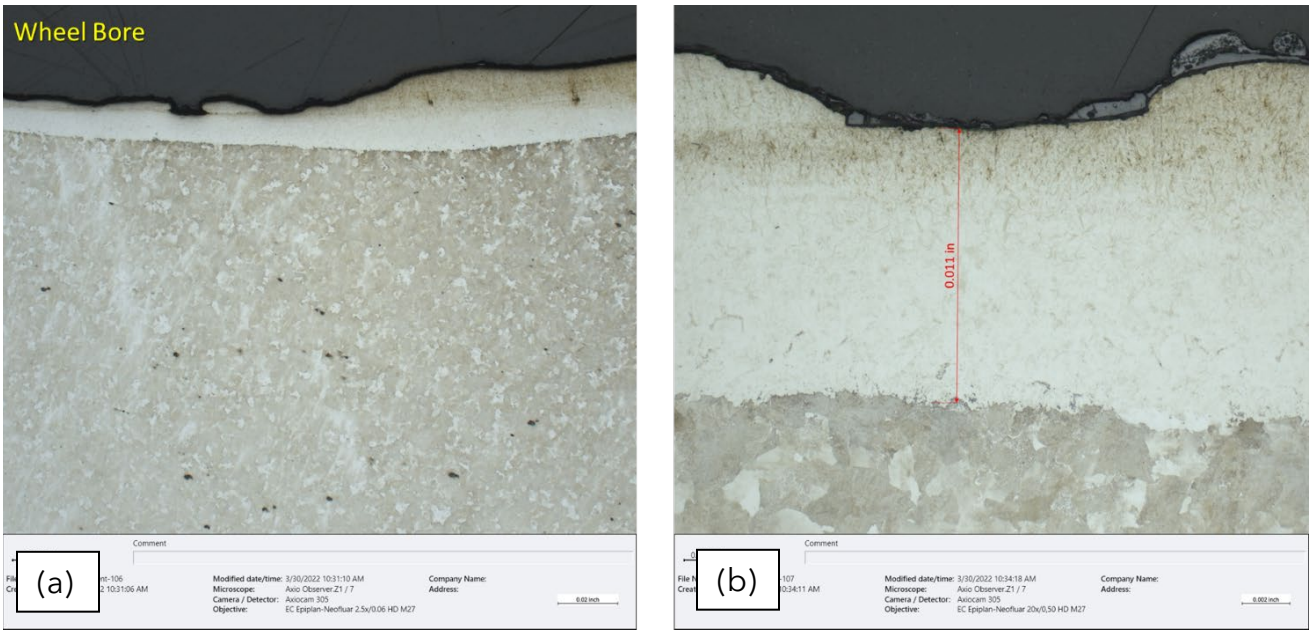

Figure 63. BF optical micrographs of the wheel bore towards the outboard edge, at (a) ~25X and (b) ~200X (etched 2% nital).

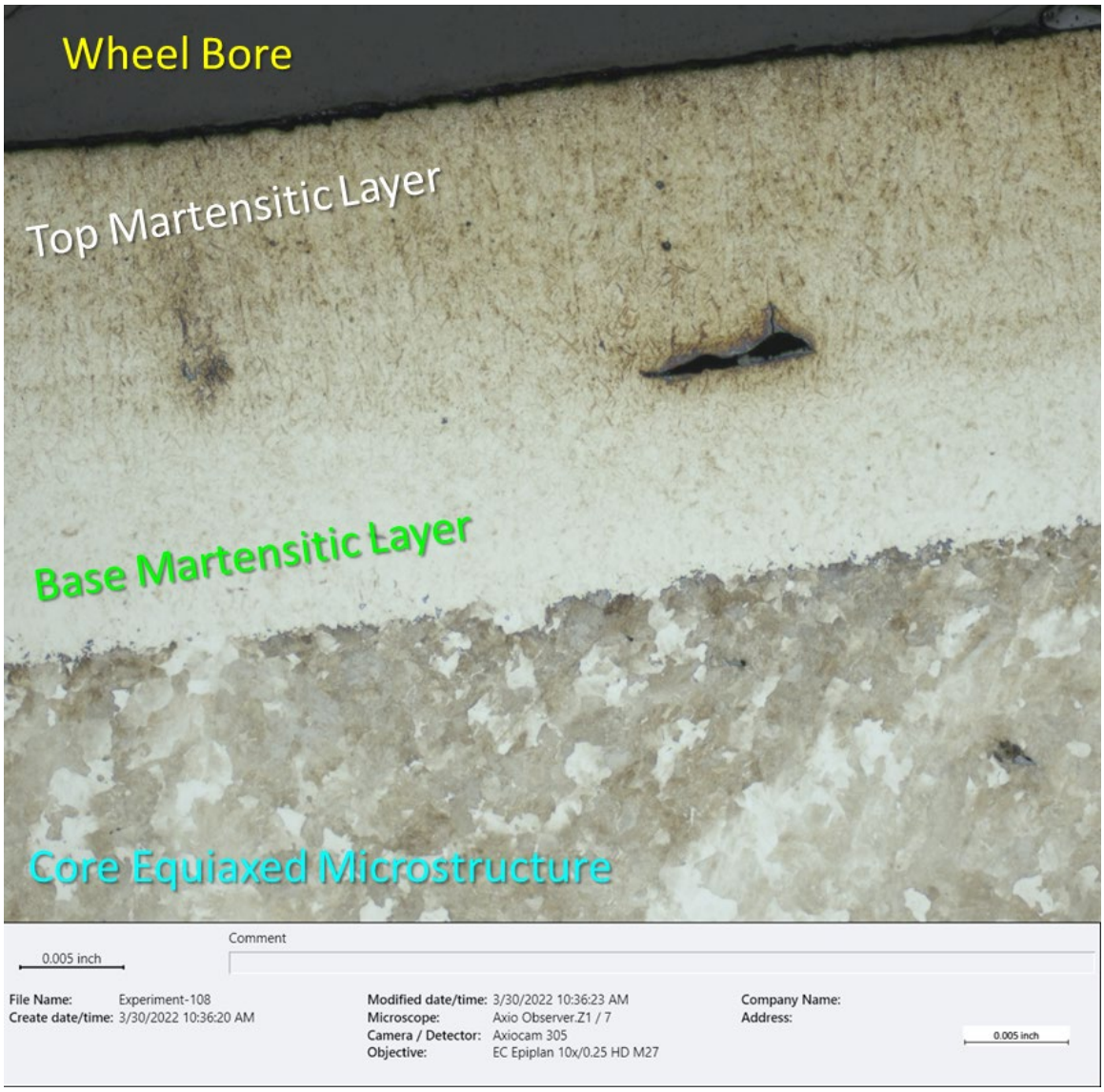

Figure 64. BF optical micrograph of the layers in Figure 63 (~100X, etched 2% Nital).

Figure 65. BF optical micrograph of the martensite layer, showing plate morphology (~500X, etched 2% Nital).

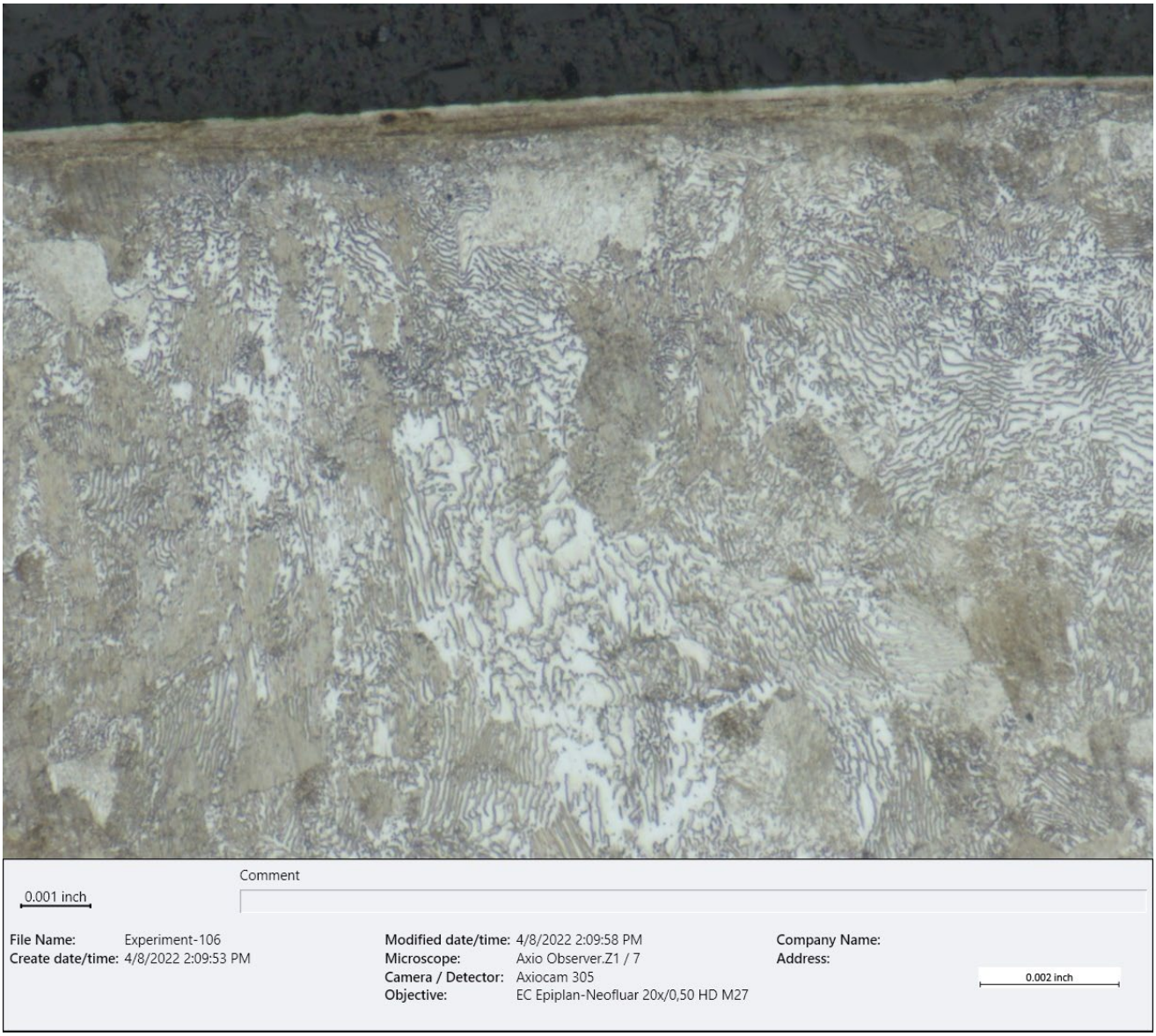

Figure 66. BF optical micrograph of the wheel bore surface, inboard from the edge, showing less surface damage and microstructural change (~500X, etched 2% nital).

Figure 67. View of the circumferential wear pattern on inboard face of the LS wheel, near the flange.

Figure 68. Closer view of the wear on the inboard face in Figure 67.

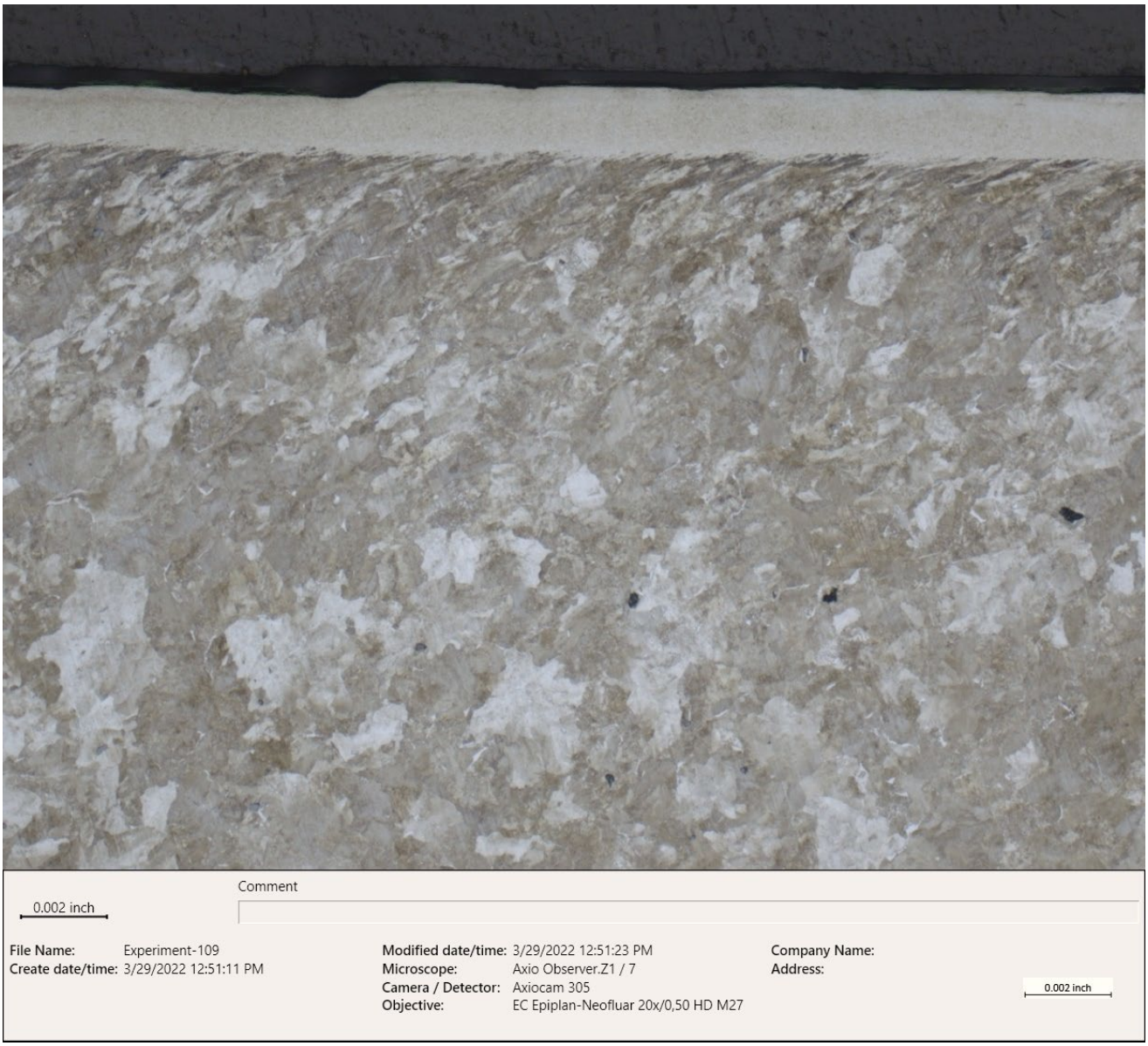

Figure 69. BF optical micrograph of surface deformation and martensite on the inboard wheel surface near the flange (~200X, etched 2% Nital).

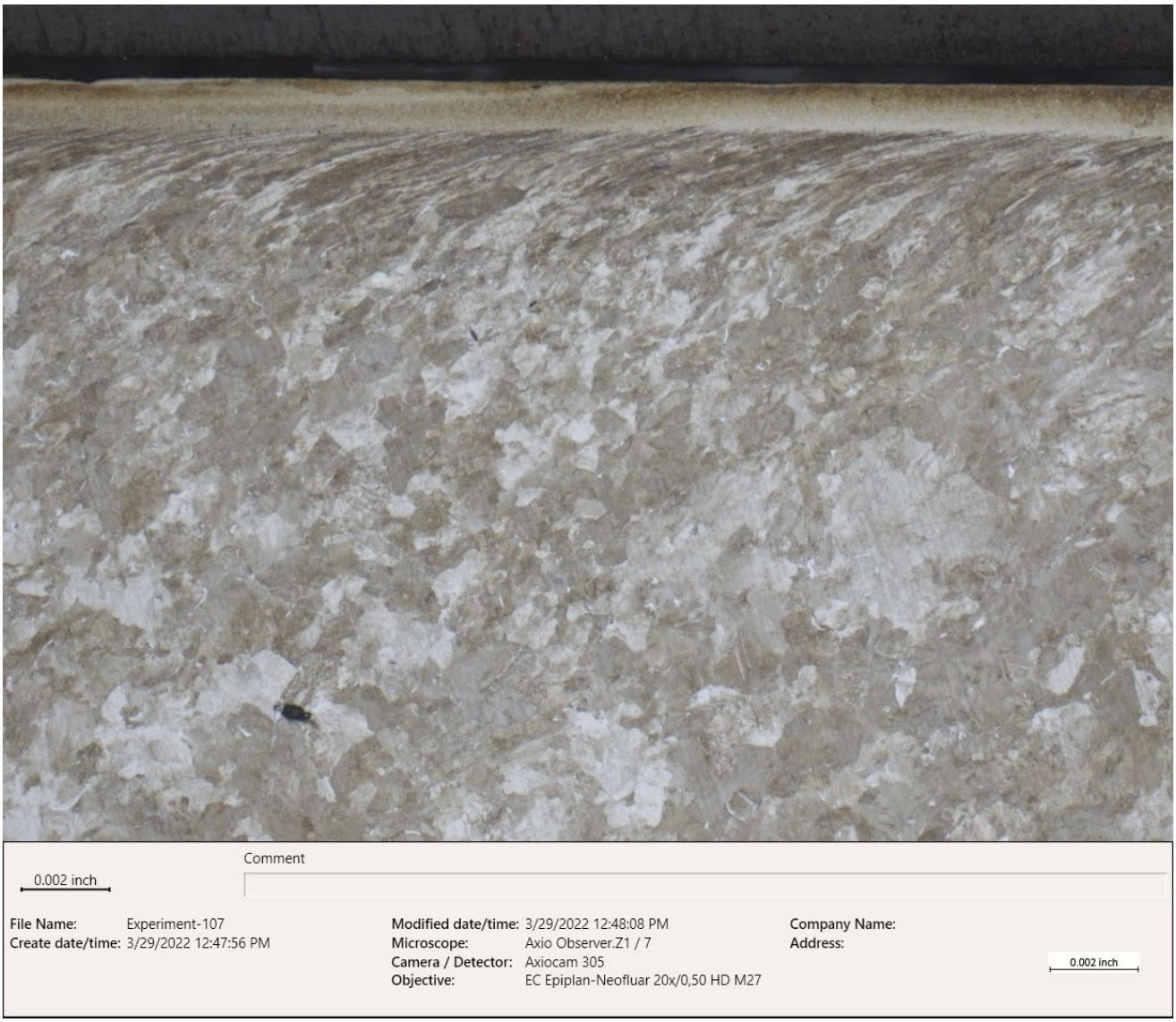

Figure 70. BF optical micrograph of another area of the inboard accident wheel surface, showing grain deformation and surface martensite (~500X, etched 2% Nital).

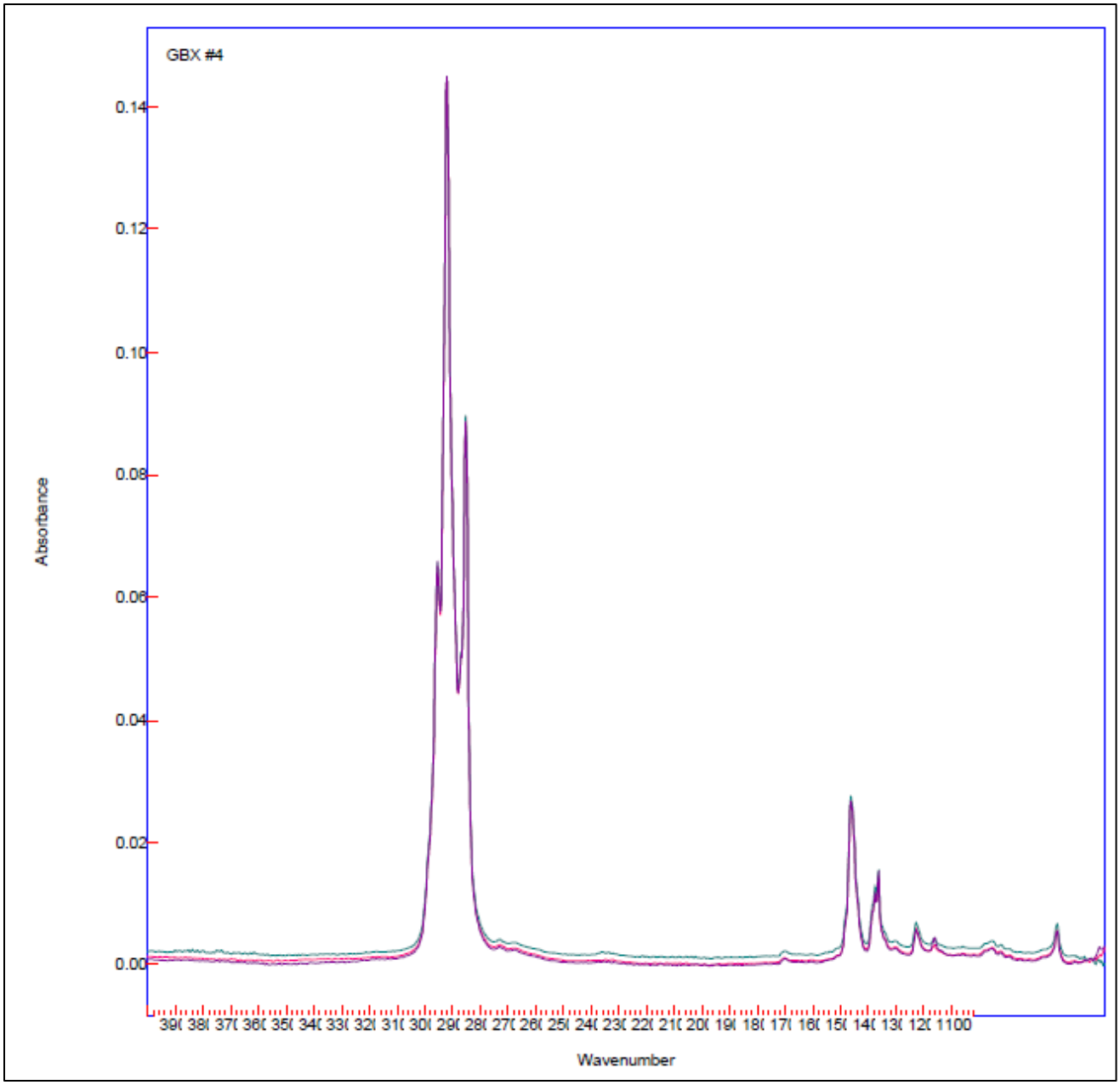

Figure 71. Overlay of FTIR spectra from the accident wheelset oil samples and an unused exemplar of the oil.